Fermi National Accelerator Laboratory

FERMILAB-Pub-85/55-T
April, 1985

Thermodynamics of QCD in the Large N Limit

L. D. McLerran and Ashoke Sen
Theoretical Physics Department
Fermilab P. O. Box 500
Batavia, IL. 60510

Operated by Universities Research Association Inc. under contract with the United States Department of Energy

Abstract: We study the thermodynamics of QCD in the limit of a large number of colors. It is argued that in this limit there is an order parameter for confinement, which is the energy density itself. We show that at a first order confinement-deconfinement phase transition, the ratio of the latent heat of the phase transition to the energy density of matter in the hadronic phase is infinite. We explicitly study the t' Hooft model of two dimensional QCD. It is shown that that at any finite temperature, the thermodynamic potential is not computable in perturbation theory, and that the high temperature limit of the thermodynamic potential is infinite in the limit of zero interaction strength. We also demonstrate how the Feynman graphs for the thermodynamic potential may be resummed to produce the same contribution as that from a resonance gas of hadrons, and show that the thermodynamic potential which is nominally of order N is in fact of order 1. We argue that at an infinite temperature, $T \sim (N\sigma)^{1/2}$, where σ is the string tension, the system may become a deconfined gas of quarks, but that there need be no phase transition at any finite temperature.

Section 1. Introduction

The physics of finite temperature and baryon number density phase transitions has been the subject of much recent numerical and analytical studies.[1] Much qualitative information has been abstracted from this analysis, but many fundamental questions still lack a satisfactory theoretical understanding. For example, it is not known whether fermions destroy the confinement-deconfinement phase transition of Yang-Mills theory in the absence of fermions, although the most recent Monte-Carlo computations lend numerical support to the thesis that the phase transition is not destroyed.[2-4] The relation between the chiral restoration phase transition and the confinement-deconfinement is not understood, although the most recent Monte-Carlo data suggest that these transitions are one and the same.[5] The latent heat of the phase transition is measured and is large when expressed in terms of the energy density of the matter below the phase transition.[6-7] There is at least an order of magnitude jump, and for practical purposes, the energy density and pressure jump from essentially zero to values typical of an ideal quark-gluon gas at the phase transition.

Another problem which is poorly understood is the reliability of perturbation theory for the computation of physical quantities at finite temperature. Linde showed that the thermodynamic potential may not be computed in perturbation theory beyond a certain fixed order in a weak coupling expansion.[8] In four dimensions, this order is g^5 for the thermodynamic potential. The breakdown of a perturbation expansion is signalled by infrared singularities. It is widely believed that the thermodynamic potential is reliably estimated up to this order, and the uncertainties in higher orders are small at high temperatures where the coupling strength is weak. The nature of the thermodynamic potential when these infrared singularities are properly accounted for is not yet fully understood.

In an attempt to throw some light on these problems, we have

considered QCD in the large N limit[9]. In this limit, some qualitative features of the numerical Monte-Carlo simulations are easily understood. As we shall soon see, bulk quantities such as the thermodynamic potential itself provide an order parameter for the confinement-deconfinement phase transition. In the deconfined and confined phases of the system, the thermodynamic potential is of order N^2 and of order one respectively. If the confinement-deconfinement phase transition is first order, the latent heat of the phase transition is infinite, when expressed as a ratio to the energy density below the phase transition, so that the transition is strongly first order. If the transition is second order, in a finite temperature interval above the transition, the energy density changes by an infinite amount compared to the energy density below the transition, and so the transition is in this sense strongly second order. At the phase transition, the large N expansion breaks down.

In an attempt to glean more insight into the structure of QCD in large N, we have studied QCD in large N in two space-time dimensions, that is the t' Hooft model. In this model, we shall show that for any finite temprature, quarks are always confined into bound hadronic states, but at an infinite temperature, $T \sim (N\sigma)^{1/2}$, where σ is the string tension, the system may become deconfined. In the high temperature limit, $(N\sigma)^{1/2} >> T >> \sigma^{1/2}$, the thermodynamic potential may not be computed in perturbation theory and is divergent in the limit $\sigma \to 0$. This non-analyticity of the weak coupling expansion is a consequence of infrared divergences, and violates the naive expectation of asymptotically free perturbation theory that the thermodynamical potential should be computable in a systematic weak coupling expansion.

We show in detail how in the confining phase, the thermodynamic potential for the theory expressed in terms of bound hadronic states arises from Feynman diagrams expressed in terms of quarks and gluons. We prove an interesting theorem, which may be useful in other contexts, which shows that if the

thermodynamic potential is projected into a color singlet sector, the momentum integrations corresponding to relative momenta of quarks in bound state wavefunctions may be directly converted from summations over Matsubara frequencies to continuous Euclidian integrations. Under weak assumptions about the nature of the bound state wavefunctions, these continuous integrations may be Wick rotated into Minkowski space, and the Feynman diagrams may be expressed in terms of Minkowski space wavefunctions. This theorem makes possible the relation between quark-gluon Feynman diagrams and a sum over hadronic resonances for the thermodynamic potential.

In the summary, we finally discuss how corrections to the large N limit may affect our conclusions. We also attempt to isolate the peculiarities of our conclusions which arise from studying two dimensions rather than four.

Section 2: General Features of Thermodynamics in Large N

The most obvious consequence of confinement is that not all the degrees of freedom of Yang-Mills theory are manifest in the set of physically accessible states. For example, there are N^2-1 colored and 1 singlet state associated with two fermions in the fundamental representation of SU(N). Only the singlet state is realized in nature, as a consequence of confinement. In the large N limit[9], the number of inaccessible colored states approaches infinity relative to the number of singlet states.

In a finite temperature and baryon number density system, this simple observation has far reaching and amusing consequences[10-11]. (Although many of the results that we shall discuss in this section have already been discussed in Ref.10, we include them here for the sake of completeness). At high temperatures, if there is a confinement-deconfinement phase transition, the number of degrees of freedom of the system must change by an infinite amount. The entropy, pressure, and energy density at some finite temperature above the confinement-deconfinement temperature must be infinite compared to that below this temperature. If the phase transition is first order, the latent heat is in this sense infinite, and if the transition is second order, the transition is in this sense infinitely strong second order. These bulk quantities themselves therefore play the role of order parmaters, and the concept of a confinement- deconfinement phase transition is well defined.

The sense in which the latent heat of the confinement-deconfinement phase transition becomes infinite may be understood by considering the thermodynamic potential in the deconfined phase at very high temperatures. At such temperatures, asymptotically free perturbation theory suggests that the thermodynamic potential is given by the two diagrams shown in Fig. 1. These diagrams give ideal gas contributions for N^2-1 gluons and N_fN quarks, where N_f is the number of quark flavors,

$$\Omega \propto \{ 2\times(N^2-1) + 4\times(7/8)\times N_f N \} T^4 \qquad (1)$$

For any finite temperature T, the thermodynamic potential is infinite as $N \to \infty$. Below the phase transition, the system is described by a color singlet hadronic gas, and the thermodynamic potential is therefore of order one as $N \to \infty$.

We therefore see that the confinement-deconfinement phase transition might generate an infinite change in the bulk properties of the system. In reaching this conclusion, we have implicitly assumed that this phase transition occurs at finite temperature even in the infinite N limit. If this is not the case, then the arguments presented above clearly do not apply since at an infinite temperature, the bulk properties may become infinite without a singularity. Let us assume for example that in the infinite N limit there is either no deconfining phase transition or that the transition occurs at a temperature $T \sim N^p$ ($p>0$). Asymptotically free perturbation theory may be a numerically accurate approximation at large temperatures in these finite N theories, but the temperature at which this approximation becomes good approaches infinity as $N \to \infty$. As a result, when we consider the $N \to \infty$ limit of these theories, asymptotically free perturbation theory is never a valid approximation at any finite temperature, and there need not be any infinite change in the thermodynamic potential of the system at a finite temperature.

In the two dimensional t' Hooft model which we shall study either the system never becomes deconfined, or deconfinement is realized only at infinite temperature. The asymptotically free perturbation theory is never valid at any finite temperature, at least in the large N limit. This is probably not the case for four dimensional theories. In four dimensions, asymptotically free perturbation theory may be a valid approximation to bulk quantities such as the thermodynamic potential at some finite temperature. This should be true even in the large N limit for $T >> \Lambda$ where Λ is a scale factor which characterizes confinement scales. Since at low temperatures, the system is a confined

hadron gas, there must be a phase transition at some finite temperature.

The difference between two and four dimensions is that the infrared behaviour of phase space is much more singular in two dimensions. For example, the first order correction to the thermodynamic potential, shown in Fig. 2, is linearly divergent. To see this, observe that the infrared singular contribution to this graph occurs for zero Matsubara frequency in the gluon line. The remaining momentum integration diverges as dk/k^2, that is linearly. In four dimensions, the first non-controllable infrared divergences occur in order g^5.

The infrared limit may be a little more severe for QCD at large N than for finite N. At finite N, the infrared singularity in Fig. 2 at zero gluon momentum may be tempered somewhat by the insertion of fermion bubbles, as shown in Fig. 3, and a temperature dependent gluon mass might be generated. If this is the case, then infrared singularities may not be a problem at least until some higher order of perturbation expansion. The severe infrared singular structure of large N QCD makes the infrared finite ideal gas contribution, Fig. 1 and Eq. 1, invalid at any finite temperature. This is a little surprising, since two dimensional QCD is a theory with a dimensional coupling constant, and conventional wisdom would say that at high temperatures the contributions to the thermodynamic potential arise from high energy quarks whose interactions are insignificant. The surprise is that the infrared interactions are what are in fact dominating the thermodynamic potential at any finite temperature. The breakdown of perturbation theory may be seen by explicitly computing the thermodynamic potential. The thermodynamic potential may be represented as a sum over meson bound states of quark-antiquark pairs. To leading order in large N, these mesons do not interact, so the sum is over non-interacting mesons.

$$\Omega = - \Sigma_i \, T \int \frac{dk}{2\pi} \ln\{1-e^{-\beta[k^2+m_i^2]^{1/2}}\} \qquad (2)$$

At high temperatures, the dominant contribution to the sum over states in Eq. 2 is for large mass mesons. Since there are a large number of these mesons, and the thermal factor does not greatly suppress the contribution of mesons with mass $m \lesssim T$, the sum over these large mass mesons is expected to give extra factors of T in Ω relative to the contribution of any single low mass meson. To see in detail how it works, we note that at large temperatures, the meson masses are

$$m_i^2 = \kappa i \alpha_s \tag{3}$$

where $\alpha_s = Ng^2/4\pi$ is the dimensional coefficient which characterizes the string tension, and κ is a constant of order one. The quark masses do not enter this relation for the large mass states which we consider. Up to a numerical constant, α_s is the string tension, $\alpha_s \sim \sigma$.

At large masses, the sum over i in Eq. 2 may be replaced by an integral. We find

$$\Omega = -T \int di \, \frac{dk}{2\pi} \, \ln\left\{1-e^{-\beta\left[k^2+\kappa\alpha_s i\right]^{1/2}}\right\} = a\,\frac{T^4}{\alpha_s} \tag{4}$$

where a is a constant of order one.

The expression for the thermodynamic potential given in Eq. 4 is appropriate for the high temperature limit of an ideal gas in four dimensions, not two. The extra powers of T may be understood to arise from the large number of states which contribute to the thermodynamic potential at large T. Also, for the contribution of a free quark gas, we expect a factor of N in the thermodynamic potential, which is absent. Notice that the thermodynamic potential is divergent in the limit $\alpha_s \to 0$. This singularity reflects the breakdown of perturbation theory in the large N limit. In general, the thermodynamic potential is singular in the limit that $\alpha_s \to 0$. In this limit, the sum over resonances is not damped by the thermal factor, and the large i contributions to the sum lead to a divergence. Put another way, by scaling, large T corresponds to small α_s, and we already have

seen that the high temperature limit is singular.

This structure of the thermodynamic potential suggests that an unconfined quark-gluon plasma might be produced at infinite temperature at infinite N, or at some temperature $T \sim \sqrt{N\alpha_s}$ for finite but large N. Recall that the thermodynamic potential for an ideal gas of quarks in two dimensions is

$$\Omega \sim NT^2 \tag{5}$$

Gluons do not contribute to the thermodynamic potential in two dimensions since there are no dynamical propagating gluons. (One degree of freedom is gauge and the other is constrained by Gauss's law.) Equations 4-5 for the thermodynamic potential agree when $T \sim \sqrt{N\alpha_s}$. Also, at this large temperature, the effect of interactions may become significant. We argued before that in calculating the partition function, the effects of interactions could be ignored, since they are suppressed by one power of N in the large N limit. As the temperature becomes large, the typical mass of a particle, which gives contribution to the partition function becomes of order T. Since the number of particles with mass$\lesssim$T is of order T^2/α_s, the density of particles grow with temperature T^2/α_s times faster than that for a gas of free particles of a single type. Due to the rapid growth of number density, the effect of multi-meson interactions becomes significant at a temperature $T\sim\sqrt{N\alpha_s}$, when the extra power of T^2/α_s compensates for the power of N^{-1} in the interaction strength.

We can now understand how a confinement-deconfinement phase transition might be dynamically realized at a finite temperature in four space-time dimensions. In four dimensions, the number of states which contribute to the partition function grow exponentially, not quadratically, as the temperature increases. In some circumstances, this exponential growth may result in an accumulation of mesons contributing to the partition function as $T \to T_c$ from below. At T_c, the number of states which contribute to the partition function would grow indefinitely, and viewed

from a world of hadrons, there would be a Hagedorn limiting temperature[12]. As the limiting temperature was approached for any finite N, the effects of multi-meson interactions would become important, and the large N expansion applied to the hadronic world, would break down. Above T_c, the thermodynamic potential would become infinite when measured in terms of the thermodynamic potential below T_c. As T approached T_c from above, at some temperature singular long distance interactions among quarks would become sufficiently large, and the perturbation expansion might break down. Another possibility is that the perturbation expansion remains valid in the quark-gluon world, but there is a first order phase transition generated by the possibility that hadrons might exist as a resonance gas at much lower free energy below T_c.

It seems that as a necessary consequence of these arguments, there are two different ways to implement the large N expansion for the thermodynamic potential. In one method of expansion, a hadronic gas results. In another method of expansion, a quark-gluon plasma results. At some temperature T_c a confinement-deconfinement phase transition results, and this phase transition is just the result of one of these two methods of expansion either being appropriate or inappropriate to the temperature range of interest, that is, it is a consequence of the breakdown of one form of the large N expansion in favor of the other. The next three sections will be devoted to finding a relation between these two methods of expansion, and determining when one or the other method fails to give a correct answer for the thermodynamic potential.

Section 3: The Thermodynamic Potential in Large N

In this section, we shall derive a perturbation expansion for the thermodynamic potential. This expansion yields the ordinary Feynman graph expansion for the thermodynamic potential. It would be appropriate if there existed some range of temperature for which the system was an unconfined quark plasma. Although this result is the standard starting point for many analysis of the properties of a quark-gluon plasma in four space-time dimensions, it is never applicable in two space time dimensions. We shall then indicate how a formal resummation of the Feynman graphs may generate the thermodynamic potential in the confining phase, although a detailed derivation of this result is left for the next two sections. This result re-expresses the thermodynamic potential as a sum over bound quarks in mesons. We also indicate how the confining and the deconfining phase of any system may be understood as the result of the breakdown of one form or the other of the series expansion for the thermodynamic potential.

The thermodynamic potential is

$$\Omega = -\frac{1}{\beta V} \ln \mathrm{Tr}\, e^{-\beta H} = -\frac{1}{\beta V} \ln \int [dA d\psi d\bar{\psi}]\, e^{S} \qquad (6)$$

where A is the gluon field, ψ and $\bar{\psi}$ are the quark fields, and S is the Euclidian action confined in a semi-infinite four volume βV,

$$S = \int_0^\beta dt \int_V d^3x \left\{ -\frac{1}{4} g^{-2} F_a^{\mu\nu} F^a_{\mu\nu} - \bar{\psi}\left(\frac{1}{i}\gamma\cdot\partial - \gamma\cdot A + m\right)\psi \right\} \qquad (7)$$

with periodic (anti-periodic) boundary conditions on the gluon (fermion) fields in the time direction. The gluon chromoelectromagnetic field strength tensor is

$$F_a^{\mu\nu} = \partial^\mu A_a^\nu - \partial^\nu A_a^\mu + f_{abc} A_b^\mu A_c^\nu \qquad (8)$$

The path integral representation of Eq. 6 is not a

convenient form for our purposes. A direct expansion in terms of vacuum graphs leads to graphs with complicated combinatoric factors. A more useful form is found by differentiating the thermodynamic potential with respect to α_s,

$$g^2\alpha_s \frac{d}{d\alpha_s} \Omega = - < \frac{1}{4} F_a^{\mu\nu} F^a_{\mu\nu} > \qquad (9)$$

For simplicity we have ignored the contribution from the ghost loop, whose sole effect in the light cone gauge is to cancel the lowest order diagram involving a single gluon loop. The notation <O> for any operator O is

$$<O> = \int [dAd\psi d\bar{\psi}]\ O\ e^S \ /\ \int\ [dAd\psi d\bar{\psi}]\ e^S \qquad (10)$$

The choice of integration constant is a little tricky since in two dimensions, the limit $\alpha_s \to 0$ is singular. We shall take the integration constant for $\alpha_s \to \infty$. In this limit, the masses of all bound states diverge, unless the quarks have precisely zero mass which is a case we do not consider. The integration constant is fixed by requiring that the thermodynamic potential at infinite coupling vanishes.

In two space-time dimensions, it is always possible to choose an axial gauge for which the gluon interactions vanish. In an axial gauge, there is only one field A and $f_{abc}A_bA_c$ is zero. We shall always work in such a gauge. The derivative of the thermodynamic potential may therefore be expressed in terms of only the full gluon propagator.

This expression for the derivative of the thermodynamic potential is best expressed in momentum space. With the free inverse gluon propagator as

$$D^{-1}_{(0)}{}^{\mu\nu}(q) = i\{q^2 g^{\mu\nu} - q^\mu q^\nu\} \qquad (12)$$

and the full propagator as

$$D^{\mu\nu}(q) = -ig^{-2} \int d^2x\ \ e^{iq\cdot x}$$

$$[<A^{\mu}(x)A^{\nu}(0)>-<A^{\mu}(x)><A^{\nu}(0)>] \qquad (13)$$

the thermodynamic potential is given as

$$\alpha_s \frac{d}{d\alpha_s} \Omega = -\frac{1}{2} \beta^{-1} \Sigma_{q_0} \int \frac{dq_1}{(2\pi)} D^{-1}_{(0)}{}^{\mu\nu}(q)$$
$$[D_{\nu\mu}(q) + \frac{(2\pi)^2}{i} g^{-2} \delta^{(2)}(q) <A_{\mu}><A_{\nu}>] \qquad (14)$$

This contribution is a vacuum Feynman graph and is shown in Fig. 4.

The leading order contribution to the 1/N expansion for Ω is given by the graphs shown in Fig. 5. These planar diagrams give a contribution of order N in the deconfined phase. A heuristic way to avoid this problem in two dimensional QCD is to re-sum the gluon insertions, and express this contribution in terms of the fermion propagator computed to leading order in the large N limit. The quark propagator is shown in Fig. 6 in terms of the irreducible quark self-energy kernel. The contributions of leading order in N to the self energy kernel Σ, which we shall call $\Sigma_{(1)}$ and which yield the propagator $S_{(1)}$ are shown in Fig. 7. The contribution to the thermodynamic potential is expressed in terms of $S_{(1)}$ as shown in Fig. 8. This graph may be thought of as vanishing since the two fermion lines which appear correspond to the dressed propagation of quarks. If the self-energy insertion is computed with an infra-red regulator, the self-energy insertion leads to infinite mass quarks, and there would be no contribution to the diagram of Fig. 8. The problem with this heuristic argument is that it is not gauge invariant. In suitable gauges, the self-energy insertion is perfectly finite. Also, a direct evaluation in light cone gauge shows that although there may be an infinite self-energy insertion with some choices of infra-red regulation, the singularity may be removed by a shift of the fermion momentum. Hence the high momentum contribution of the loop integrals for Fig. 8 cancels this mass singularity.

In the next section, we shall show that this contribution truly vanishes in the confined phase, by considering the partition function properly evaluated as a sum over gauge invariant states. At this point in our classification of diagrams, we shall assume that this is in fact the case, and consider the next leading contributions in the large N limit. It is these contributions which are of zero order in N as N approaches infinity, and should therefore give the resonance sum in the confined phase. As we shall see later, these graphs sum up to give the contributions shown in Fig. 9. In this figure, T is the connected scattering matrix element for quark-antiquark scattering. In the next section, we shall explicitly see how in this diagram, scattering of quarks and anti-quarks sum up to give a sum over finite energy color singlet meson states, as shown in Fig.10. It is plausible that this might occur given the structure of Fig. 9. The scatterings generate bound state poles, with residues which are the bound state wavefunctions. Again, there are several problems with this heuristic argument. One problem is that these wavefunctions are evaluated with Euclidian momentum, and it is not obvious how to analytically continue this momentum to Minkowski space. It is also not clear at this stage how the sum over frequencies gets converted to continuous integrations over momenta of the bound state wavefunctions. Finally, note that although the graphs of Fig. 9 (b)-(c) have the same structure as those of Fig. 9 (a), we are forced to write these as separate contributions because of the combinatoric factors. It will also be shown in the next section, that this mysterious combination is precisely what is required to yield the derivative of Ω, with the mysterious factors arising from differentiating the meson mass with respect to α_s.

It is not yet clear how there might be two different methods of summing the thermodynamic potential in four dimensions, both of which are valid in large N, for the confined and unconfined phases of the theory. We shall show in Secs. 4-5 that the thermodynamic potential expressed as a sum over bound states, or

as a sum over the constituent quark and gluon states may be realized as two different limits of the same formal Feynman diagram expansion. We derive the Feynman rules of the system with quarks and gluons as internal lines, taking into account the fact that in calculating Tr $e^{-\beta H}$, we sum over only those states of the bulk matter which are color singlets.[13] In the thermodynamic limit, this constraint becomes irrelevant and we recover the usual Feynman rules[14]. This limit reproduces the correct partition function of the system in the deconfined phase. This calculation is no longer valid in the confined phase, and we believe that this is signalled by uncurable infrared divergences of the individual Feynman graphs. Instead, we compute the amplitude by taking the $N \to \infty$ limit before taking the thermodynamic limit. This limit is expected to produce the correct result in the confined phase, since the spectrum of bound states is independent of N in the large N limit, and all the interaction terms vanish in the same limit. We shall show in Secs. 4-5 that in this same limit, the Feynman graphs expressed in terms of the quark and gluon lines may be rearranged to reproduce the thermodynamic potential as a sum over bound states. This calculation is no longer valid in the deconfined phase, and we expect the breakdown to be signalled by a divergence in the sum over bound states, as implied by a Hagedorn spectrum of bound states.

We now explain in some detail how these two limits differ in the actual computation of the thermodynamic potential. In order to impose the color singlet constraint on the bulk system, we must first expand the partition function in terms of the usual connected and disconnected Feynman diagrams, use the rules of Sec. 4 to project out the color singlet part of each diagram. and then try to exponentiate the answer. Let us analyze the contribution represented in Fig. 11a. Although the contribution shown in Fig. 11a may be shown to vanish due to the color singlet constraint, the contribution from disconnected diagrams shown in Fig. 11b do not vanish if the number of such diagrams are of the order of N or larger than N. In fact, the

color singlet constraint becomes irrelevant when the number of such diagrams is large compared to N. Since the contribution shown in Fig. 11a is proportional to its volume, and the major contribution in the expansion $e^x = \Sigma\, x^n/n!$ comes from $n \sim x$ for large x, we may conclude that the contribution to the exponential associated with the contribution shown in Fig. 11a will come from diagrams of the form shown in Fig. 11b with the total number of disconnected diagrams of order $\beta V\Lambda^2$, Λ being the typical mass scale of the theory. As a result, in the thermodynamic limit for a fixed N, we may ignore the color singlet constraint, and the leading contribution to the partition function is given by the exponential of Fig. 11a.

In computing the thermodynamic potential in the confining phase, however, we take the $N \to \infty$ limit before the thermodynamic limit. Then using the color singlet constraint, we may show that the contribution to the partition function from any diagram of the form of Fig. 11b is at most of order unity, and not of order N. As a result, the thermodynamic potential is of order unity. As we shall show in the next section, the thermodynamic potential calculated in this way may also be identified with that calculated from the sum over the mesonic bound states of the large N limit.

Physically, these results may be understood as follows: Fig. 10 gives the dominant contribution to the thermodynamic potential if the thermal media provides enough shielding to produce quarks which propagate freely for times large compared to the typical particle interaction times. This happens in the deconfined phase. In the confined phase, a quark cannot propagate freely unless it is paired with an anti-quark of opposite charge. Hence only that part of Fig. 11b which corresponds to the propagation of a color singlet bound state of a quark anti-quark pair contributes to the partition function.

Section 4 Color singlet projection

In this section, we shall continue the discussion of the thermodynamic potential. We shall carefully implement the color singlet constraint on the states in the partition function, by expressing the thermodynamic potential as a sum over color singlet multiquark states. We then derive the Feynman rules for evaluating the thermodynamic potential. In the next section we shall show how these Feynman rules give an expression for the thermodynamic potential in terms of the bound states.

If we allow the states $|n\rangle$ appearing in

$$e^{-\beta V\Omega} = \Sigma_n \langle n| e^{-\beta H}|n\rangle \tag{15}$$

to be arbitrary multi-quark states, then the Feynman rules for evaluating Ω are the standard ones. The Feynman graphs are evaluated with Euclidian metric, and energies are replaced by Matsubara frequencies with the discrete values $(2p+1)\pi/\beta$ for fermions and $2p\pi/\beta$ for bosons.

We shall, however restrict the sum in Eq. 15 to color singlet states. As we shall soon see, the Feynman rules for evaluating quantities with this constraint are somewhat different than those without the constraint. We accomplish the color singlet constraint by making use of the color singlet projection operator[13]. Let U represent a color rotation generated by the group element g. The color singlet partition function is

$$e^{-\beta V\Omega} = \int [dg]\ \Sigma_p \langle p| e^{-\beta H}\ U(g)|p\rangle \tag{16}$$

[dg] is the properly normalized Weyl measure which projects out color singlet states.

For any element of a group g it is always possible to find another element g' such that

$$U(g')U(g)U(g'^{-1}) = U_d(g) \tag{17}$$

is diagonal. Since H commutes with all the color generators, we have

$$\Sigma_p \langle p| e^{-\beta H} U(g)|p\rangle = \Sigma_p \langle p| U^{-1}(g') e^{-\beta H} U_d(g) U(g')|p\rangle$$
$$= \Sigma_p \langle p| e^{-\beta H} U_d(g)|p\rangle \qquad (18)$$

If Q_i denote the diagonal generators of the U(N) gauge group, then we have

$$\mathrm{Tr}\ e^{-\beta H} U_d(g) = \mathrm{Tr}\ e^{-\beta H} e^{i\alpha_i Q_i} \qquad (19)$$

where α_i are the parameters characterizing the invariance class of the group element g. Eq. 16 may therefore be written as

$$e^{-\beta V \Omega} = \int [d\alpha]\ \mathrm{Tr}\ e^{-\beta H} e^{i\alpha_i Q_i} \qquad (20)$$

Since all the diagonal generators commute with H and with themselves, the integrand of Eq. 20 may be evaluated by replacing H with an effective Hamiltonian

$$H' = H - i\alpha_i Q_i \qquad (21)$$

Let us choose for convenience the generator Q_i in such a way that all its diagonal entries except the i'th one is zero. The i'th fermion state is defined as the column vector whose only non-vanishing entry is the i'th row. The i'th anti-fermion is the conjugate of the i'th fermion.. The [i,j] gluon state is the state with the same quantum numbers as the combination of the i'th fermion and j'th anti-fermion. The operator $\Sigma_j \alpha_j Q_j$ gives α_i/β, $-\alpha_j/\beta$, and $(\alpha_i-\alpha_j)/\beta$ acting on the i'th fermion, j'th anti-fermion, and (i-j)'th gluons states respectively. The Feynman rules for the color singlet partition function of Eq. 19 are now easy to derive. Note first that the extra term $i\Sigma_j \alpha_j Q_j/\beta$ is quadratic in the fields, and therefore contributes only to the propagators of the various fields and not their

vertices. The propagators differ from the usual propagators in Euclidian momentum space in the following way. For the i'th fermion propagator carrying momentum k, the discrete variable k^o, which takes the values $(2n+1)\pi/\beta$, is replaced by $k^o - \alpha_i/\beta$ everywhere in the propagator. Similarly, the [i- j]'th gluon carrying momentum k^o is modified by making the substitution $k^0 \to k^0-(\alpha_i-\alpha_j)/\beta$ everywhere in the propagator.

With these Feynman rules, we now analyze the thermodynamic potential given by Eq. 19. We first analyze the diagrams of order N shown in Fig. 5. Consider the lowest order contribution represented in Fig. 2. This contribution may be written as

$$\Omega_A = (2\pi/\beta)^2 \sum_{k^o_{1,2}=(2n_{1,2}+1)\pi/\beta} \int dk_1 dk_2 \{(k_1^o-\alpha_i/\beta)^2+k_1^2+m^2\}^{-1}$$

$$\{(k_2^o-\alpha_j/\beta)^2+k_2^2+m^2\}^{-1} f(k_1^o-\alpha_i/\beta, k_2^o-\alpha_j/\beta) \qquad (22)$$

where f denotes the contribution from the fermion numerators and the gluon propagators. Ths equation may be re-written as

$$\Omega_A = \int_c dt_1 dt_2 \{(t_1-\alpha_i/\beta)^2+k_1^2+m^2\}^{-1}\{(t_2-\alpha_j/\beta)^2+k_2^2+m^2\}^{-1}$$

$$f(t_1-\alpha_i/\beta, t_2-\alpha_j/\beta) \quad \frac{1}{2}\beta \cot\{\frac{\beta t_1}{2} - \frac{\pi}{2}\} \quad \frac{1}{2}\beta \cot\{\frac{\beta t_2}{2} - \frac{\pi}{2}\} \qquad (23)$$

where the contour in the complex t plane is taken for each t integration as is shown in Fig. 12. Defining new integration variables as

$$t_1' = t_1-\alpha_i/\beta \qquad (24)$$

$$t_2' = t_2-\alpha_j/\beta \qquad (25)$$

Eq. 23 becomes

$$\Omega_A = \int_c dt_1 dt_2 \frac{1}{t_1^2+k_1^2+m^2} \frac{1}{t_2^2+k_2^2+m^2} f(t_1,t_2) \frac{\beta}{2} \cot\{\frac{\beta t_1}{2} - \frac{\pi}{2} + \frac{\alpha_i}{2}\} \frac{\beta}{2} \cot\{\frac{\beta t_2}{2} - \frac{\pi}{2} + \frac{\alpha_j}{2}\} \quad (26)$$

where we have dropped the primes from the new variables t'_1 and t'_2. For the part of the contour integration in the t_1 plane where Im $t_1 > 0$, we expand

$$\cot\{\frac{\beta t_1 - \pi + \alpha_i}{2}\} = -i \frac{1-e^{i(\beta t_1+\alpha_i)}}{1+e^{i(\beta t_1+\alpha_i)}} = -i \{1-e^{i(\beta t_1+\alpha_i)}\} \Sigma_{m=0}^{\infty} (-1)^m e^{im(\beta t_1+\alpha_i)} \quad (27)$$

The sum is convergent for Im $t_1 > 0$. For Im $t_1 < 0$, we expand as

$$\cot\{\frac{\beta t_1 - \pi + \alpha_i}{2}\} = i \frac{1-e^{-i(\beta t_1+\alpha_i)}}{1+e^{-i(\beta t_1+\alpha_i)}} = i (1-e^{-i(\beta t_1+\alpha_i)} \Sigma_{m=0}^{\infty} (-1)^m e^{-im(\beta t_1+\alpha_i)} \quad (28)$$

The cotangent term involving t_2 may be expanded in entirely the same manner. The part of the integrand which depends upon β and α_i, $i = 1, \cdots, N$ is therefore a sum of terms of the form

$$e^{im_1\beta t_1} e^{im_2\beta t_2} e^{im_1\alpha_i} e^{im_2\alpha_j} \quad (29)$$

where $-\infty < m_1 < \infty$ and $-\infty < m_2 < \infty$. The traces over the fermion loops require that we must sum over the i and j independently from 1 - N. (This is most easily seen using the double line representation for the gluon propagator.) The result of this summation is to sum over i and j on the terms shown in Eq. 29. Since all of the α dependence is in this term, the rest of the integrand may be taken outside the α integral, and we have to evaluate the expression

$$\int [d\alpha] e^{im_1\beta t_1} e^{im_2\beta t_2} \Sigma_{i=1}^{N} e^{im_1\alpha_i} \Sigma_{j=1}^{N} e^{im_2\alpha_j} \quad (30)$$

If we had not imposed the color singlet constraint, there would not have been an α integral in Eq. 29, and all of the α's would be set to zero. The summations in Eq. 30 would then yield N^2. Combining one factor of N into the factor of g^2 which multiplies Fig. 2, this diagram would be of order N. We shall show that,

$$\int [d\alpha] \; \Sigma \; e^{im_1\alpha_i} \; \Sigma \; e^{im_2\alpha_j} = |m_1| \; \delta_{m_1,-m_2} + N^2 \delta_{m_1,0} \; \delta_{m_2,0} \quad (31)$$

For m_1 and m_2 not both zero, this diagram is of 1/N and is non-leading compared to the magnitude of the color singlet meson contributions. On the other hand, the contribution for $m_1 = m_2 = 0$ has no dependence on β. This contribution affects only the vacuum energy and may be ignored for our purposes.

The contribution from higher order diagrams with one fermion loop as given by Fig. 8, may be similarly shown to be non-leading except for the vacuum contribution. This is done by using the result, discussed in Appendix A,

$$\int [d\alpha] \; \Sigma_{i_1} \; e^{im_1\alpha_{i_1}} \; \Sigma_{i_2} \; e^{im_2\alpha_{i_2}} \cdots\cdots \; \Sigma_{i_r} e^{im_r\alpha_{i_r}} = 0, \; r \text{ odd} \quad (32)$$

$$= \Sigma_{\text{permutations}} \; |m_1| \; |m_3| \cdots\cdots |m_{r-1}| \; \delta_{m_1,-m_2}$$

$$\delta_{m_3,-m_4} \cdots\cdots \delta_{m_{r-1},-m_r}, \; r \text{ even} \quad (33)$$

if none of the m_k's vanishes. If some of the m_k are zero, then the sum over each of the corresponding α's gives a factor of N. The contribution of the remaining terms may be carried out using Eqs. 32-33. The summation is over all pairings from the set of $m_1, \cdots\cdots m_r$. Since only the term with all of the m's set to zero, which is a vacuum contribution, is non-vanishing in the large N limit, we conclude that the graphs of Fig. 8 are non-leading relative to the meson contribution.

We now discuss the contribution associated with two fermion

loops as shown in Fig. 9. The contribution from these graphs is at most of order unity. A typical graph with two fermion lines contributing is shown in Fig. 13. The contribution may be written as

$$\Sigma_{p^o} \int dp \int [d\alpha] \Sigma_{k_1^o} \cdots \Sigma_{k_r^o} \Sigma_{i_1=1}^{N} \cdots \Sigma_{i_r=1}^{N} f(k_1^0+\alpha_{i1}/\beta, \cdots k_r^0+\alpha_{ir}/\beta, k_1, \cdots k_r, p^0, p) \tag{34}$$

where k denotes the spatial component of the loop momentum.

Note that some of the color indices in Fig. 13 are constrained to be equal due to group theory factors. Also in the fermion propagators, $\alpha_{i\ell}/\beta$ is added to the momenta k_ℓ^o but is subtracted from the momenta $p^o-k_\ell^o$. This is because the momentum $p-k_\ell$ flows along the arrow while the momenta k_ℓ flows against the arrow. As a result, $\alpha_{i\ell}$ and k_ℓ^o always appear in the combination $k_\ell^o + \alpha_{i\ell}/\beta$. We may now express Eq. 34 as

$$\int [d\alpha] \Sigma_{p^o} \int dp \int_C (\Pi_{\ell=1}^{r} dt_\ell) f(t_1, \cdots t_r, k_1, \cdots k_r, p^0, p)$$

$$\Pi_{\ell=1}^{r} \Sigma_{i\ell=1}^{N} \cot\left\{\frac{\beta t_\ell - \pi + \alpha_{i\ell}}{2}\right\} \tag{35}$$

We may expand the cotangent as we did in the previous analysis. Since to start with, the contribution was of order unity, the only way we may get a contribution of order unity after the α integrals is to set $m_i=0$ in each expansion. This is equivalent to setting the cotangent to unity in Eq. 35, or in other words, replacing the summation over the Matsubara frequencies k_ℓ^o by continuous integration over Euclidian momenta. Only for the momenta p^o must a discrete frequency sum remain.

We have to this point concentrated only on connected diagrams. We must also treat disconnected diagrams since it is the expression for Z, which contains connected as well as disconnected diagrams, and not ln Z ($=-\beta V\Omega$), which contains only

connected diagrams, over which the α integrations are directly performed. We shall now discuss how the disconnected diagrams sum up when a global color singlet constraint is included. To study this, we must first expand Z in terms of connected and disconnected diagrams, do the α integrals, and then sum up the result. We shall show that the total contribution from the connected and the disconnected diagrams which survive the α integrations may be written as e^S, where S is the sum of the connected diagrams integrated over α and a new class of diagrams which we shall discuss below.

First consider disconnected diagrams of the type shown in Fig. 14. Contributions from these diagrams may be analyzed in the same way as the contributions from Fig. 8. We may bring the contribution from the disconnected diagrams into the form

$$\int_C \Pi_\ell dt_\ell dk_\ell \int [d\alpha] \quad F(t) \; \Pi_\ell \{ \Sigma_{i\ell=1}^{N} \cot\{\frac{\beta t_\ell - \pi + \alpha_{i\ell}}{2}\}\} \qquad (36)$$

The cotangent functions may be expanded as in Eqs. (27) and (28). The integrand is given by a sum of terms of the form

$$\int [d\alpha] \; e^{i\Sigma_{\ell=1}^{r} m_\ell t_\ell} \; \Pi_{\ell=1}^{r} \{ \Sigma_{i\ell=1}^{N} e^{i m_\ell \alpha_{i\ell}} \} \qquad (37)$$

This contribution may be analyzed using Eq. 32 and 33. The largest contribution to Eq. 37 comes when all the m's are zero. Combined with the explicit powers of 1/N in the coupling constant, this gives a contribution of order N^2. This is simply the square of the O(N) vacuum energy term, since this contribution is obtained simply by replacing all the internal energy sums in Fig. 14 by continuous integrals. The next order contribution is of order unity, and is found by replacing all of the m's except two by zero. Let m_i and m_j be the only two nonzero components. This contribution may be evaluated using Eq. 31. There are two cases. If both m_i and m_j come from the same bubble in Fig. 14, then the contribution factorizes into a product of O(N) vacuum energy diagram and an O(1/N) contribution to the partition function from the connected diagram represented

in Fig. 8. This is therefore not a new contribution to ln Z, and is already included in the disconnected diagrams which sum up to yield the clustered expression for Z. On the other hand if m_i and m_j come from the different bubbles in Fig. 14, the contribution may no longer be interpreted as a higher order term in the expansion of $e^{\ln Z}$, and must be included in ln Z as a new contribution. Diagrammatically, we shall represent these contributions as disconnected bubbles with one loop from each bubble connected by a dotted line to represent which of the m's are taken to be non-zero. A typical example is shown in Fig. 15.

When we consider higher order diagrams containing more disconnected bubbles, we may expect to get more new terms in the expression for ln Z. We shall now show that this does not happen. Let us consider a set of disconnected diagrams. The contribution from these diagrams may be expressed as in Eq. 36. The leading contribution is of order N^p which comes from setting all the m's to zero in Eq. 37. This term may be trivially identified with the p'th power of the O(N) contribution to the vacuum energy in the p'th order of expansion of $e^{\ln Z}$. The next order contribution is of order N^{p-2}, which is obtained from setting two of the m's to be non-zero. If these two m's come from the same bubble, the contribution may be identified with the pruduct of the $O(N^{p-1})$ contribution from the (p-1)'th power of the vacuum contribution and the O(1/N) contribution to ln Z from Fig. 8. If the two m's come from different bubbles, the contribution is identified with the product of the $O(N^{p-2})$ contribution from the (p-2)'th power of the vacuum energy and the O(1) contribution from the graphs of Fig. 15.

The only potentially new contribution to ln Z may come from graphs with four or more m's non-zero. The only non-factorizing contribution (which may not be expressed as products of terms already in ln Z) come from terms of the form shown in Fig 16, where the dotted lines connect the loops for which the m's are non-zero. The m's at the two ends of a dotted line are paired according to Eq. 33. We lose four powers of N from each of

these graphs since four of the m's are non-vanishing. As a result, the contribution from Fig. 6a is of order $1/N^2$ and that of Fig. 6b is of order $1/N$. These graphs do not therefore contribute to ln Z to order unity.

Finally, we want to demonstrate that the combinatoric factors associated with each graph works out to correctly exponentiate the graphs. We shall see that this works in an example, and not construct a full proof. This example consists of graphs with 2p disconnected bubbles, and we want to pick up the terms where each of the disconnected bubbles is paired with another bubble, thus giving the p'th power of the graphs shown in Fig. 15. The combinatoric factor desired of this graph is $1/p!$, whereas the original graph has a factor of $1/2p!$. There are however $(2p!)/\{p!2^p\}$ ways of pairing 2p objects, hence the net combinatoric factor is $1/\{p!2^p\}$. Absorbing the factor of 1/2 in the definition of the graphs shown in Fig. 15, we see that we indeed get the correct combinatorial factor needed for exponentiation. Also, by using the structure of Eq. 33, we see that the contribution from the term with 2p disconnected bubbles may indeed be identified with the p'th power of the contribution with two disconnected bubbles, because of the factorized form of the right hand side of Eq. 33.

This indicates the proof that the total contribution to ln Z exponentiates, with the terms in the exponential containing the vacuum energy terms, contributions of the form shown in Fig. 13 with all the k^o's being integrated over a continuous range from $-\infty$ to ∞, while the p^o is summed over the discrete Matsubara frequencies $2\pi n/\beta$ and contributions of the form shown in Fig. 15. In actual practice, we shall however evaluate $\alpha_s\, d/d\alpha_s\, \Omega$ instead of Ω. This differential may be written as

$$\alpha_s\, d/d\alpha_s\, \Omega = -\frac{1}{Z} \int [d\alpha] \sum_n \langle n| e^{-\beta H + i\alpha_j Q^j} (4g^2)^{-1} \mathrm{Tr}\, F_{\mu\nu} F^{\mu\nu} |n\rangle \tag{38}$$

In other words, it is the trace of the gluon propagator plus an additional contribution of the form shown in Fig. 17 d

coming from the one point gluon function. The numerator of Eq. 38 may be analyzed exactly in the same way as that of Z. It may be expressed as a product of Z and terms of the form shown in Fig. 17. In these graphs, the gluon line with a cross represents the propagator whose trace is being computed. Although in evaluating the Feynman diagrams, the crossed gluon propagator may be treated as an ordinary gluon propagator, distinguishing this gluon from the others helps us keep track of combinatoric factors. The graphs of Fig. 17 a have the same topology as those of Fig. 8 and do not contribute to order unity in the large N limit, except for trivial vacuum energy terms. Graphs in Figs. 17b-d have the same topological structure as those of Fig. 9, and may be analyzed in a similar way. As a result of the color singlet projection, all of the internal frequency sums are replaced by continuous integrals, while the overall energy carried by the quark-anti-quark pair in the color singlet channel is still summed over discrete frequencies. The graph of Fig. 17e comes from the non-factorizability of the color singlet projected disconnected vacuum diagrams, and must be included in our analysis.

Section 5

In this section, we shall analyze the sum of the diagrams shown in Figs. 17 b-e. To do this, we express the contribution from Figs. 17c-d as in Fig. 18a while half of the contribution from Fig. 17 b, together with another graph where the direction of the arrow in the lower fermion loop is reversed, may be identified to Fig. 18 b and c with the addition of some disconnected diagrams. Here, G is the full four fermion Green's function, including the self-energy insertions on the external legs. Trace over all the color indices are performed directly in Fig.17, and the factors of N obtained from these traces are combined with the factors of N in the coupling constants to give terms of order unity. Hence G does not carry any color indices, and is independent of N when expressed as a function of α_s. Σ denotes the one particle irreducible self- energy insertion on the fermion line, and S^{-1} is the full fermion propagator. We shall discuss the disconnected diagrams at the end of this section.

The 1PI fermion self-energy part involving the crossed gluon in Fig.18(b) and (c) may be identified with $-\alpha_s(\partial S^{-1}/\partial\alpha_s)$. Thus we may write the contribution to $\alpha_s\, d/d\alpha_s$ ln Z from Figs. 18 a-b as

$$\frac{L}{2}\,\Sigma_{p_o}\int\frac{dp}{2\pi}\;\frac{id^2k_E}{(2\pi)^2}\,\frac{id^2q_E}{(2\pi)^2}\,G_E(p,q_E,k_E)\;\alpha_s d/d\alpha_s\;\{\;I(p,q_E,k_E) - K(p,q_E,k_E)\;\} \qquad (39)$$

where the subscript E refers to the Euclidian momentum and L is the length of the box. The factors of i multiplying d^2k_E and d^2q_E, and the factor of i^{-1} multiplying $\delta(q_E-k_E)$ is due to euclidean nature of these momenta, and will disappear once we Wick rotate the integrals to the Minkowski space. Here

$$K = \frac{(2\pi)^2}{i}\,\delta(q_E-k_E)\;S^{-1}(p-q_E)\;S^{-1}(q_E) \qquad (40)$$

and

$$I = -4\pi\alpha_s \gamma^\mu \times \gamma^\nu i D^{(0)}_{\mu\nu}(q-k) \tag{41}$$

is the kernel of the Bethe-Salpeter equation. The first γ matrix in this expression operates on the fermon line, and the second γ matrix operates on the anti-fermion. $D^{(0)}_{\mu\nu}(k)$ is the free propagator for a gluon of momentum k.

The Greens function G(p,q,k) may be expressed as

$$G(p,q,k) = i \Sigma_n \Psi_n(p,q) \frac{1}{p^2-M_n^2+i\epsilon} \Psi^*_n(p,k) \tag{42}$$

where M_n is the mass of the n'th bound state, Ψ_n is the corresponding wavefunction,

$$\Psi_n(p,q) = \int d^2x\, d^2y\, e^{-ip\cdot x_e - i(p-q)\cdot y} \langle n,p|T(\Psi^\dagger(x)\Psi(y))|0\rangle \tag{43}$$

and Ψ^*_n is the complex conjugate of a similar expression with the time ordering replaced by anti-time ordering. The wavefunctions Ψ_n satisfy the normalization condition[15]

$$-i \int \frac{d^2k}{(2\pi)^2} \frac{d^2q}{(2\pi)^2} \Psi^*_n(p,q)\, \alpha_s d/d\alpha_s \{K(p,q,k)-I(p,q,k)\}$$

$$\Psi_n(p,k) = \alpha_s d/d\alpha_s\, M_n^2 \tag{44}$$

In Eq. 39, the integrals over q and k as well as over the internal momenta in G are in Euclidian space. We shall however Wick rotate the integration contour to convert them into Minkowski space integrals. We may then drop the subscripts E from Eq. 39. Substituting for G from Eq. 42 and using Eq. 44, we may write Eq. 39 as

$$\frac{L}{2} \Sigma_{p_o} \int \frac{dp_1}{2\pi} \Sigma_n \alpha_s \frac{dM_n^2}{d\alpha_s} \frac{1}{p^2-M_n^2+i\epsilon} =$$

$$- \frac{L}{2} \, d/d\alpha_s \, \Sigma_n \, \Sigma_{p_o} \int \frac{dp_1}{2\pi} \, \ln(-p^2+M_n^2-i\varepsilon) \qquad (45)$$

Since Eq. 39 is the expression for $\alpha_s d/d\alpha_s \ln Z$, we see that $\ln Z$ may be identified as

$$- \frac{L}{2} \, \Sigma_n \, \Sigma_{p_o} \int \frac{dp}{2\pi} 1 \ln(-p^2+M_n^2-i\varepsilon) \qquad (46)$$

which is exactly the result we expect for a gas of free particles of masses M_n ($n = 1 \cdot\cdot \infty$)

Let us now consider the contribution from the disconnected diagrams. In the original set of graphs, there were a set of disconnected diagrams of the form shown in Fig. 17 e. While identifying the set of graphs shown in Fig. 17 b to those of Fig. 18b and c, we get another set of disconnected diagrams. These two sets do not cancel. However, there may be other contributions to the disconnected diagrams which are potentially ambiguous. This is due to the fact that in deriving Eq. 45 from Eq. 39, we had to interchange the summation over an infinite number of bound states with integration over the relative momenta q and k. Let us for example note that G satisfies the integral equation

$$G(p,q,k) = \int \frac{d^2\ell_1}{(2\pi)^2} \frac{d^2\ell_2}{(2\pi)^2} K(p,q,\ell_1) \, I(p,\ell_1,\ell_2) \, G(p,\ell_2,k) + K(p,q,\ell_1) \qquad (47)$$

while each of the Ψ's satisfies the homogeneous equation

$$\Psi_n(p,q,k) = \int \frac{d^2\ell_1}{(2\pi)^2} \frac{d^2\ell_2}{(2\pi)^2} K(p,q,\ell_1) \, I(p,\ell_1,\ell_2) \, \Psi_n(p,\ell_2,k) \qquad (48)$$

As a result, if in Eq. 47 we substitute for G using Eq. 42, interchange the limits Σ_n and $\int d^2\ell_2$, the left and right hand sides are equal only up to the addition of the disconnected piece K.

Since, at present, we do not have an unambiguous method to extract the disconnected piece that emerges while interchanging

the two limits, we are unable to show that the total contribution from disconnected diagrams vanishes. Since the contributions to ℓnZ from disconnected diagrams are, however, proportional to L^2, instead of L, as is the case for the connected diagrams, we believe that the contribution is unphysical and must cancel in the end.

Before concluding this section, we shall give another derivation of the equivalence of Eq. 39 and Eq. 45 for two dimensional QCD. Let I_1 and I_2 denote the contributions from Fig. 18a-b respectively before performing the dp_1 integration and the frequency sum. Ignoring the contribution from the disconnected pieces, we may write,

$$I_1 = \frac{1}{2} \int \frac{d^2q}{(2\pi)^2} G(p,q,q)\ S^{-1}(p-q)\ S^{-1}(q) \tag{49}$$

$$I_2 = -\frac{1}{2} \int \frac{d^2q}{(2\pi)^2} G(p,q,q)\left(\alpha_s \frac{dS^{-1}(q)}{d\alpha_s} S^{-1}(p-q) + \alpha_s \frac{dS^{-1}(p-q)}{d\alpha_s}\right) \tag{50}$$

We shall carry out the rest of our discussion in the light cone gauge. We first summarize the main results of two dimensional QCD in the light cone gauge. In this gauge the Green's function G satisfies the integral equation

$$\begin{aligned} G(p,q,k) &= (2\pi)^2\ S(p-q)S(q)\ \delta^{(2)}(q-k) \\ &\quad - 4g'^2\ S(q)S(p-q) \int \frac{d^2\ell_1}{(2\pi)^2} D(q-\ell_1)\ G(p,\ell_1,k) \\ &= (2\pi)^2 S(p-q)S(q)\ \delta^{(2)}(k-q) \\ &\quad - S(q)\ S(p-q)\ 4g'^2\ D(q-k)\ S(k)\ S(p-k) \\ &\quad + 16g'^4\ S(q)\ S(p-q) \int \frac{d^2\ell_1}{(2\pi)^2} \frac{d^2\ell_2}{(2\pi)^2}\ D(q-\ell_1)\ G(p,\ell_1,\ell_2)\ D(k,\ell_2) \\ &\quad S(k)\ S(p-k) \end{aligned} \tag{51}$$

These equations may be diagrammatically represented as shown in Fig. 19. Here D(k) denotes the gluon propagator carrying momentum k, and g'=g/N. Also, in this gauge we may treat the fermion and the gluon fields as one component objects, with the following Feynman rules:

$$\text{Gluon propagator:}\quad D^{(o)}(q) = i\,P\,\frac{1}{(q^-)^2} \tag{52}$$

where P denotes the principal value prescription.

$$\text{Fermion propagator:}\quad S^{(o)}(p) = \frac{ip^-}{(2p^+p^- - m^2 + i\varepsilon)} \tag{53}$$

and

$$\text{Gluon-fermion vertex:}\quad -2ig\,N^{1/2} = -2ig' \tag{54}$$

The superscript (o) in Eqs. 52-53 refers to the fact that the propagators $S^{(o)}$ and $D^{(o)}$ are the tree level fermion and gluon propagators. The full fermion propagator may be written as

$$S(p) = \frac{ip^-}{(2p^+p^- - m^2 - p^-\Sigma(p) + i\varepsilon)} \tag{55}$$

where to leading order in the large N limit

$$\Sigma(p) = -\frac{g'^2}{\pi p^-} \tag{56}$$

The Bethe-Salpeter wavefunction satisfies an integral equation

$$\Psi_n(p,q) = -4g'^2 i\,S(p-q)S(q)\int\frac{d^2k}{(2\pi)^2}\,P\{\frac{1}{(k^- - q^-)^2}\}\,\Psi_n(p,k) \tag{57}$$

We define

$$\Phi_n(p,q^-) = \int dq^+\,\Psi_n(p,q) \tag{58}$$

Integrating both sides of Eq. 57 with respect to q^- we get

$$\{2p^+ - \frac{M^2}{q^-} - \frac{M^2}{p^- - q^-}\}\ \Phi_n(p,q^-) = -\frac{g'^2}{\pi}\int_o^{p^-} dk^-\ P\{\frac{1}{(k^- - q^-)^2}\}$$

$$\Phi_n(p,k^-) \qquad (59)$$

where

$$M^2 = m^2 - \frac{g'^2}{\pi} \qquad (60)$$

Since Φ_n is the wavefunction of the bound state n with mass M_n, it must be an eigenstate of the P^+ operator with eigenvalue $M_n^2/2P^-$. Equation 59 may then be written as

$$P^-\{\frac{M^2}{p^-} + \frac{M^2}{p^- - q^-}\}\Phi_n(p,q^-) - \frac{g'^2}{\pi}\int_o^{p^-} dk^-\ P\{\frac{1}{(p^- - q^-)^2}\}\Phi_n(p,q^-)$$

$$= M_n^2\ \Phi_n(p,q^-) \qquad (61)$$

The integral operator on the left hand side of Eqn. 61 may be identified with the mass operator M^2 for the bound state.

We shall now evaluate the integrals I_1 and I_2 given by Eqns. 49-50. We express I_1 as

$$I_1 = \frac{1}{2}\Sigma_n \int \frac{d^2q}{(2\pi)^2}\{S^{-1}(p-q)S^{-1}(q)\ \Psi_n(p,q)\ \frac{i}{p^2 - M_n^2}\ \Psi_n^*(p,q)\}$$

$$= \frac{1}{2}\Sigma_n \int \frac{d^2q}{(2\pi)^2}\{-\frac{ig'^2}{\pi^2}\int dk^-\ P\{\frac{1}{(q^- - k^-)^2}\}\Phi_n(p,k^-)\ \frac{i}{p^2 - M_n^2}\ \Phi_n^*(p,k^-)\} \qquad (62)$$

upon using Eq. 57. This result is however ambiguous up to the addition of disconnected diagrams. For example, if we had used Eq. 51 for G first, and then used Eq. 42 to express G as a sum over bound state wavefunctions, we would have been left with a disconnected diagram. This is the same ambiguity that was mentioned before.

We analyze I_2 by using Eq. 51 and ignoring the disconnected piece. This gives

$$I_2 = -\frac{1}{2}\alpha_s \int \frac{d^2q}{(2\pi)^2}\{S(q)\frac{dS^{-1}(p-q)}{d\alpha_s} + S(p-q)\frac{dS^{-1}(q)}{d\alpha_s}\}\ S(q)S(p-q)$$

$$\{ -4g'^2 D(0) + 16g'^4 \int \frac{d^2\ell_1}{(2\pi)^2} \frac{d^2\ell_2}{(2\pi)^2} D(q-\ell_1)\, G(p,\ell_1,\ell_2)\, D(q-\ell_2)\} \tag{63}$$

Note that the quantity D(0) entering this equation is formally infinite, but as we shall show, this term drops out of our final expression for the thermodynamic potential. Using the explicit forms for S and Σ, and performing the q^+ integral in Eq. 63, we get

$$I_2 = \frac{1}{2} \int \frac{dq^-}{(2\pi)^2} (-i\pi) \{ 2p^+ - \frac{M^2}{q^-} - \frac{M^2}{p^- - q^-} \}^{-2} \{ \frac{1}{q^-} + \frac{1}{p^- - q^-} \}$$
$$(-\frac{g'^2}{\pi}) \{ I'(0) + \int \frac{d^2\ell_1}{(2\pi)^2} \frac{d^2\ell_2}{(2\pi)^2} K(q-\ell_1)\, G(p,\ell_1,\ell_2)\, K(q-\ell_2)\} \tag{64}$$

where

$$I'(q) = -4g'^2 D(q) \tag{65}$$

On the other hand, integrating both sides of Eq. 51 over k^+ and q^+ and setting $q^- = k^-$, we obtain

$$\int dq^+ dk^+ G(p,q,k)\,|_{q^-=k^-} = (-i\pi)^2 \{ 2p^+ - \frac{M^2}{q^-} - \frac{M^2}{p^- - q^-} \}^{-2}$$
$$\{ I'(0) + \int \frac{d^2\ell_1}{(2\pi)^4} \frac{d^2\ell_2}{} I'(q-\ell_1)\, G(p,\ell_1,\ell_2)\, I'(q-\ell_2) \} \tag{66}$$

where disconnected contributions have again been ignored. Using Eqs. 64 and 66, I_2 may be expressed as

$$I_2 = -\frac{i}{2} \int \frac{dq^-}{(2\pi)^2} \frac{g'^2}{\pi^2} \{ \frac{1}{q^-} + \frac{1}{p^- - q^-} \} \int dq^+ dk^+ G(p,q,k)\,|_{k^-=q^-}$$
$$= -\frac{i}{2} \int \frac{dq^-}{(2\pi)^2} \frac{g'^2}{\pi^2} \{ \frac{1}{q^-} + \frac{1}{p^- - q^-} \} \Sigma_n \Phi_n(p,q^-) \frac{i}{p^2 - M_n^2} \Phi_n^*(p,q^-) \tag{67}$$

We therefore find that

$$I_1 + I_2 = \frac{1}{2\pi} \Sigma_n \int dq^- \{ -\frac{g^2}{\pi} \{ \frac{1}{q^-} + \frac{1}{p^- - q^-} \} \Phi_n(p,q^-)$$

$$+ \frac{g^2}{\pi} \int dk^- \, \Phi_n(p,k^-) \Big\} \frac{1}{p^2-M_n^2} \Phi_n^*(p,q)$$

$$= -\frac{1}{2\pi} \Sigma_n \int dq^- \, \Phi_n^*(p,q^-) \frac{1}{p^2-M^2} g^2 \frac{d}{dg^2} \left\{ \frac{M^2}{p^-} \right\} \Phi_n(p,q^-)$$

$$= \frac{1}{2\pi} \Sigma_n \int dq^- \frac{1}{p^-} \Phi_n^*(p,q^-) \left\{ g^2 \frac{d}{dg^2} \ln \{-p^2+M^2+i\varepsilon\} \right\} \Phi_n(p,q^-) \tag{68}$$

Using the completeness of the functions Φ_n and the normalization condition derived from Eq.(3.8) of Ref.15,

$$\int dq^- \, \Phi_n^*(p,q^-) \, \Phi_n(p,q^-) = -\delta_{mn} p^- \pi \tag{69}$$

we get

$$I_1+I_2 = -\alpha_s \frac{d}{d\alpha_s} \Sigma_n \ln \{-P^2+M^2+i\varepsilon\} \tag{70}$$

The net contribution to $\alpha_s \frac{d}{d\alpha_s} \ln Z$ is given by

$$\alpha_s \frac{d}{d\alpha_s} \ln Z = -\frac{L}{2} \alpha_s \frac{d}{d\alpha_s} \Sigma_{p^o} \int \frac{dp_1}{2\pi} \ln \{-P^2+M^2+i\varepsilon\} \tag{71}$$

We finally find therefore

$$\ln Z = -\frac{L}{2} \Sigma_{p^o} \int \frac{dp_1}{2\pi} \Sigma_n \ln \{-P^2+M_n^2+i\varepsilon\} \tag{72}$$

which is precisely the expected result for a set of non-interacting scalar mesons.

In the integration with respect to g^2 which gives Eq. 64, there is a g independent integration constant which has been implicitly chosen to be zero. This constant is specified by properly reproducing the strong coupling result which must consist of the contribution of the lowest mass bound state of the theory. This contribution is properly included in the result of Eq. 72.

Section 6. Summary and conclusion

In this paper we have analyzed the thermodynamics of QCD in the large N limit. In this limit, the contribution to the thermodynamic potential in the confining and the deconfining phase are of order unity and N^2 respectively. We show how these two results may be realized as two different limits of the same formal Feynman diagram expansion, which is obtained by restricting the sum over states in the partition function to be over gauge invariant states only. The result for the thermodynamic potential in the deconfining phase, which we expect to be given by the asymptotically free perturbation theory, is obtained if we take the thermodynamic limit before taking the large N limit. On the other hand, the result for the thermodynamic potential in the confining phase is obtained if in the same perturbation expansion, we take the large N limit before taking the thermodynamic limit, and formally resum the perturbation expansion. We believe that the confining-deconfining phase transition corresponds to the breakdown of one or the other limit, as we approach the phase transition temperature from different directions.

Although we have focussed our attention on the two dimensional 't Hooft model, we believe that the general results mentioned above are valid even for four dimensional QCD in the large N limit. The two dimensional QCD, however, has some special features which we do not expect to generalize to four dimensions. In the two dimensional theory, asymptotically free perturbation theory is never a valid expansion. This is signalled by severe infrared divergences which occur in the perturbation expansion if we take the thermodynamic limit before taking the large N limit. On the other hand, if we take the large N limit before taking the thermodynamic limit, we get the thermodynamic potential as a sum over meson bound states. The sum is finite all finite values of temperature, and hence is expected to give the correct answer for the thermodynamic

potential at all temperatures. This is presumably not the case for four dimensional QCD in the large N limit. The asymptptically free perturbation expansion suffers from infrared divergences only at some high order in perturbation theory, and is expected to give the correct answer for the thermodynamic potential at sufficiently high temperature. Also, the thermodynamic potential in the confining phase, expressed as a sum over meson bound states, may not be well defined for all values of temperature, due to the existence of a Hagedorn limiting temperature. As a result, different methods of expansion, as mentioned before, must be used to calculate the thermodynamic potential in different ranges of temperature.

Acknowledgements: We wish to thank W. Bardeen, S. Das, S. Elitzur, R. Pisarski, M. Polikarpov, J. Schmidt and L. Wilets for enlightening discussions.

Appendix A

We want to calculate the quantity

$$\Omega^{-1} \int [dg]\ \mathrm{Tr}_f\, g^{m_1}\ \mathrm{Tr}_f\, g^{m_2} \cdots \mathrm{Tr}_f\, g^{m_r} \qquad (A.1)$$

in an SU(N) gauge group. Here g denotes an element of SU(N), and $m_1, m_2, \cdots m_r$ are integers satisfying $\Sigma_{i=1}^{r} m_i = 0$ and $\Sigma_{i=1}^{r} |m_i| < N$. Tr_f denotes the trace in the fundamental representation, [dg] is the Weyl measure for SU(N) and Ω is the volume of SU(N). The operation $\Omega^{-1}\int [dg]$ counts the number of singlet representations contained in the integrand.

Our conjecture is that the result of Eq. A.1 when none of the m's are zero is given as

$$0 \quad \text{if } r \text{ is odd}$$

$$\Sigma_{\text{all pairings}} |m_1|\ |m_3| \cdots |m_{r-1}|\ \delta_{m_1+m_2,0}\ \delta_{m_3+m_4,0} \cdots \delta_{m_{r-1}+m_r,0} \quad \text{if } r \text{ is even} \qquad (A.2)$$

If some of the m's are zero, the corresponding trace gives a factor of N, and the remaining contribution may be evaluated using Eq. A.2.

The verification of this conjecture is begun by parameterizing g by its N eigenvalues $t_1, \cdots, t_N$ satisfying $\Pi_{i=1}^{N} t_i = 1$. t_i's are related to the parameters α_i's introduced in the text through the relation $t_i = e^{i\alpha_i}$. Eq. A.1 may therefore be written as

$$\Omega^{-1}\int [dt]\ \{\Sigma_{i_1=1}^{N} t_{i_1}^{m_1}\}\ \{\Sigma_{i_2=1}^{N} t_{i_2}^{m_2}\} \cdots \{\Sigma_{i_r=1}^{N} t_{i_r}^{m_r}\} =$$

$$\Omega^{-1}\int [dt]\ \left[\frac{\partial}{\partial a_1} \cdots \frac{\partial}{\partial a_r}\ \exp\left\{\Sigma_{s=1}^{r} a_s\, \Sigma_{i=1}^{N} t_i^{m_s}\right\}\right]_{a_1=a_2=\cdots=a_r=0} \qquad (A.3)$$

The exponenial in Eq. A.3 may be written as

$$\Pi_{i=1}^{N} \exp\{ \Sigma_{s=1}^{r} a_s t_i^{m_s} \} \tag{A.4}$$

We now evaluate Eq. A.3 using a result derived in Ref. 16. For our purposes, the result may be stated as follows. If G(t) is a function of t with the expansion

$$G(t) = \Sigma_{n=-\infty}^{\infty} A_n t^n \tag{A.5}$$

then

$$\Omega^{-1} \int [dt] \Pi_{i=1}^{N} G(t_i) = \det D \tag{A.6}$$

where

$$D_{k\ell} = A_{k-\ell} \tag{A.7}$$

In our case

$$G(t) = \exp \{ \Sigma_{s=1}^{r} a_s t^{m_s} \} \tag{A.8}$$

The non-zero entries in D are for k,ℓ satisfying

$$k-\ell = \Sigma_{s\in\theta} m_s \tag{A.9}$$

where θ is any subset of the set $\{1,\cdots,r\}$. The corresponding value of $D_{k\ell}$ is $\Pi_{s\in\theta} a_s$. D also has non-zero entries at $k-\ell = \Sigma_{s\in\theta} n_s m_s$ where n_s are positive integers larger than unity. These terms will contain more than one power of some of the a's and will not contribute to Eq. A.3 after setting all the a's to zero.

Now define the matrix B as

$$D = I + B \tag{A.10}$$

B has the same structure as D with the diagonal identity elements removed. We may therefore write

$$\text{Det } D = \exp \text{Tr ln } \{I + B\} = \exp \{ \Sigma_{n=1}^{\infty} \frac{(-1)^{n+1}}{n} \text{ Tr } B^n \}$$

$$= \Sigma_{p=0}^{\infty} \{ \Sigma_{n=1}^{\infty} \frac{(-1)^{n+1}}{n} \text{ Tr } B^n \}^p \frac{1}{p!} \qquad (A.11)$$

According to Eq. A.3, the coefficient of the $\Pi_{s=1}^{r} a_r$ term in Eq. A.11 gives the result for Eq. A.1. In evaluating Eq. A.11, we must find the diagonal element of B^n. A typical diagonal element of B^n has the form

$$B_{i_1 i_2} B_{i_2 i_3} \cdots B_{i_n i_1} \qquad (A.12)$$

The non-zero values in Eq. A.12 are obtained if

$$\begin{aligned} i_1 - i_2 &= \Sigma_{s<\theta_1} m_s \\ i_2 - i_3 &= \Sigma_{s<\theta_2} m_s \\ &\vdots \\ i_n - i_1 &= \Sigma_{s<\theta_n} m_s \end{aligned} \qquad (A.13)$$

where $\theta_1, \cdots \theta_n$ are subsets of the set $\{1, \cdot\cdot, r\}$. We also want them to be mutually exclusive in order to avoid two or more powers of a single a_s. The corresponding contribution to Eq. A.12 is given by

$$\Pi_{\ell=1}^{n} \{\Pi_{s<\theta_\ell} a_s\} \qquad (A.14)$$

Eq. A.13 yields

$$\Sigma_{\ell=1}^{n} \Sigma_{s<\theta_\ell} m_s = 0 \qquad (A.15)$$

The diagonal elements of B^n are therefore sums of products of a_s's. A particular product in the sum contains those a_s's whose

corresponding m_s's add up to zero.

Let $P_1, \cdots P_k$ be all possible subsets (not necessarily mutually exclusive) of the set $(1, \cdots, r)$ such that

$$\Sigma_{s \subset P_\ell} m_s = 0 \quad \text{for all } \ell = 1, \cdots, k \tag{A.16}$$

Then,

$$\Sigma_{n=1}^{\infty} \frac{(-1)^{n+1}}{n} \text{Tr } B^n = \Sigma_\ell G(R_\ell, \{m_s;\ s \subset P_\ell\}\ \Pi_{s \subset P_\ell} a_s \tag{A.17}$$

where R_ℓ is the number of elements in the set P_ℓ. $G(R_\ell, \{m_s; s \subset P_\ell)$, by definition, is the coefficient of $\Pi_{s \subset P_\ell} a_s$ in the expansion of the left hand side of Eq.(A.17). It is evaluated by setting all the a_s's outside the set P_ℓ to zero, and counting the coefficient of $\Pi_{s \subset P_\ell} a_s$ on the left hand side of Eq. A.17. Our conjecture is that

$$G = 0 \qquad \text{for all } R_\ell > 2$$

$$G = |m_1|\ \delta_{m_1, -m_2} \quad \text{for } R_\ell = 2 \tag{A.18}$$

We shall soon describe how to verify this conjecture. But first we shall show that Eq. A.18 leads to Eq. A.2. To see this, note that due to Eq.(A.18), the only way a particular a_s may appear in Eq. A.17 is that its corresponding m_s has a negative counterpart. In other words, the set $\{m_1, \cdots, m_r\}$ must be of the form $\{m_1, -m_1, m_3, -m_3, \cdots m_{r-1}, -m_{r-1}\}$. We find upon using Eqs. A.17-A.18 that

$$\Sigma_{n=1}^{\infty} \frac{(-1)^{n+1}}{n} \text{Tr } B^n = \{|m_1| a_1 a_2 + |m_3| a_3 a_4 + \cdots |m_{r-1}| a_{r-1} a_r\} \tag{A.19}$$

The coefficients of $a_1 \cdots a_r$ on the right hand side of Eq. A.11 are therefore given by

$$|m_1|\ |m_3| \cdots |m_{r-1}| \tag{A.20}$$

which proves Eq. A.2.

We shall now illustrate how we verify the conjecture of Eq. A.18. Let us denote the elements of the set $\{m_s, s \subset P_\ell\}$ by $M_1, \cdots M_{R_\ell}$ and the corresponding a's by $A_1, \cdots A_{R_\ell}$. The quantity G is evaluated by determining the coefficient of $\Pi_{s=1}^{R_\ell} A_s$ on the left hand side of Eq. A.17. Since this may be done by setting all the elements of the set $\{a_1 \cdots a_r\}$ to zero, except the ones belonging the set P_ℓ, we see that G depends only on R_ℓ and the set $\{M_1, \cdots M_{R_\ell}\}$, but not on r or the other members of the set $m_1, \cdots m_r$. As a result, we may evaluate $G(r,\{m_1, \cdots m_r\})$ by setting $P_\ell = \{m_1, \cdots m_r\}$, and then computing $G(R_\ell,\{M_1, \cdots M_{R_\ell}\})$ for arbitrary R_ℓ and $M_1, \cdots M_{R_\ell}$ by setting $r = R_\ell$ and the set $\{m_1, \cdots m_r\}$ to be $\{M_1, \cdots M_{R_\ell}\}$.

In order to calculate $G(r,\{m_1, \cdots m_r\})$, we need to evaluate the coefficient of $\Pi_{i=1}^{r} a_i$ in Eq. A.12 and then add them up with a weight factor of $(-1)^n/n$. The sets θ_ℓ in Eq. A.13 must the satisfy

$$U_{\ell=1}^{n} \theta_\ell = \{m_1, \cdots m_r\} \tag{A.21}$$

Each term in Eq. A.12 is therfore associated with a particular division of a set of r objects into n boxes, with each box containing at least one object. The permutations of the objects inside a box θ_ℓ are irrelevant, whereas the permutations of the boxes θ_ℓ are relevant. In other words, the contributions to Eq. A.12 is different if instead of Eq. A.13, we have

$$\begin{aligned} i_1 - i_2 &= \Sigma_{s \subset \theta_2} m_s \\ i_2 - i_3 &= \Sigma_{s \in \theta_1} m_s \\ &\cdot \\ &\cdot \\ &\cdot \\ i_r - i_1 &= \Sigma_{s \subset \theta_r} m_s \end{aligned} \tag{A.22}$$

For a particular choice of the sets $\theta_1,\cdots\theta_n$ and a fixed ordering of the sets, all the differences i_1-i_2 , $\cdots i_r-i_1$ are fixed, but i_1 is still arbitrary. Let the matrix B be of dimension NxN where N is a number much larger than $|m_1|$, $\cdots|m_r|$. Then the number of possible values of i_1 is given by N - $\max(i_\ell-i_k)$, where max $(i_\ell-i_k)$ denote the maximum difference batween any two i_ℓ's in the set $(i_1,\cdots,i_n)$ determined by Eq. A.22.

The coefficient of N in G is therefore determined from the number of ways r objects may be divided into n distinguishible boxes, each box containing at least one object. If $I_n(r)$ denotes this number, then the coefficient of N in G is given by

$$\Sigma_{n=1}^{r} \frac{(-1)^{n+1}}{n} I_n(r) \tag{A.23}$$

I_n may be evaluated by using the following recursion relation,

$$I_n(r) = n^r - \Sigma_{\ell=1}^{n-1} \binom{n}{\ell} I_{n-\ell}(r) \tag{A.24}$$

$$I_1 = 1 \tag{A.25}$$

Eq. A.24 reflects the fact that the total number of ways to put r objects in n ordered boxes with each box containing at least one object is the difference between the total number of ways to put r objects in n boxes and the total number of ways to put r objects in n boxes with at least one box containing no object.

We have evaluated I_n using Eqs. A.24-25 and verified that Eq. A.23 vanishes for $r \leq 20$. The evaluation of the N independent part is more difficult. At present we know of no other way to calculate it other than to explicitly generate all permutations, calculate $\max(i_k-i_1)$ for all of them, and add the permutations up with the proper coefficients. We have done this for $r \leq 8$, with randomly generated $m_1,\cdots,m_r$ satisfying $\Sigma\, m_s = 0$. The answer is zero in all cases except for r = 2, in which case it is $|m_1|$. Our conjecture is therefore verified for $r \leq 8$.

References:

1. See for example, Proceedings of Quark Matter '83, held at Brookhaven National Lab., Sept.26-29, 1983, Nucl. Phys. A418; Proceedings of Quark Matter '84, held at Helsinki, Finland, Jun. 17-21, 1984; E. Shuryak, Phys. Rep. 61, 71 (1980).

2. R. Gavai, M. Lev and B. Peterson, Phys. Lett. 140B, 397 (1984).

3. J. Polonyi, H. Wyld, J. Kogut, J. Shigemitsu and D. Sinclair, Phys. Rev. Lett. 53, 644 (1984).

4. F. Fucito, S. Solomon and C. Rebbi, Nucl. Phys. B248, 615 (1984); F. Fucito, R. Kinney and S. Solomon, Caltech report No. CALT-68-1189 (1984).

5. F. Fucito, R. Kinney and S. Solomon, Ref.4.

6. T. Celik, J. Engels and H. Satz, Phys. Lett. 129B, 323 (1983); B. Svetitsky and F. Fucito, Phys. Lett. 131B, 165 (1983).

7. J. Kogut, H. Matsuoka, M. Stone, H. Wyld, S. Shenker, J. Shigemitsu and D. Sinclair, Phys. Rev. Lett. 51, 869 (1983).

8. A. D. Linde, Phys. Lett. 96B, 289 (1980).

9. See for example, S. Coleman, Lectures delivered at the Erice summer school (1980), S. Das, to appear in Rev. Mod. Phys.

10. C. B. Thorn, Phys. Lett. 99B, 458 (1981).

11. A. Gocksch and F. Neri, Nucl. Phys. B224, 81 (1983); R. D. Pisarski, Phys. Rev. D29, 1222 (1984).

12. R. Hagedorn, Nuovo Cimento Suppl. 3, 147 (1965).

13. L. Turko, Phys. Lett. 104B, 153 (1981); K. Redlich and L. Turko, Z. Phys. C5, 201 (1980).

14. H.-Th. Elze, W. Greiner and J. Rafelski, Phys. Lett. 124B, 515 (1983), M. I. Gorenstein, O. A. Mogilevsky, V. K. Petrov and G. M. Zinovjev, Z. Phys. C13, (1983), M. I. Gorenstein, S. I. Lipskikh, V. K. Petrov and G. M. Zinovjev, Phys. Lett. 123B, 437 (1983).

15. N. Nakanishi, Suppl. Prog. Theor. Phys. No. 43, 1969).

16. A. B. Balantekin, J. Math. Phys. 25, 2028 (1984).

Figures:

Fig. 1 The ideal gas contribution to the thermodynamic potential for a) quarks and b) gluons.

Fig. 2 The first order contribution to the thermodynamic potential.

Fig. 3 Insertion of fermion bubbles in the first order correction to the thermodynamic potential.

Fig. 4 The thermodynamic potential in terms of the full gluon propagator.

Fig. 5 The leading contribution to the thermodyanamic potentail in the large N limit.

Fig. 6 The quark propagator in terms of the fermion self energy kernel.

Fig. 7 The leading order contributions to Σ

Fig. 8 The leading order contribution to Ω expressed in terms of S_1

Fig. 9 The contribution to Ω of order 1 in the large N expansion. T is the quark-antiquark scattering matrix in this expression.

Fig. 10 A sum over meson states for the thermodynamic potential.

Fig. 11 Unclustered vacuum graphs which have singlet projections and may contribute to Ω.

Fig. 12 The contour integration for Eqn. 23.

Fig. 13 A typical graph involving two fermion loops which contributes to the thermodynamic potential.

Fig. 14 One type of disconnected diagram which contributes to the color singlet partition function.

Fig. 15 A typical diagram which is a residue of a disconnected diagram after a color singlet projection is taken.

Fig. 16 New, non-factorizing contributions to the color singlet partition function arising from disconnected vacuum graphs.

Fig. 17 Some disconnected vacuum graphs.

Fig. 18 The leading order graphs which in the large N limit yield a resonance sum.

Fig. 19 The Bethe-Salpeter equation for G.

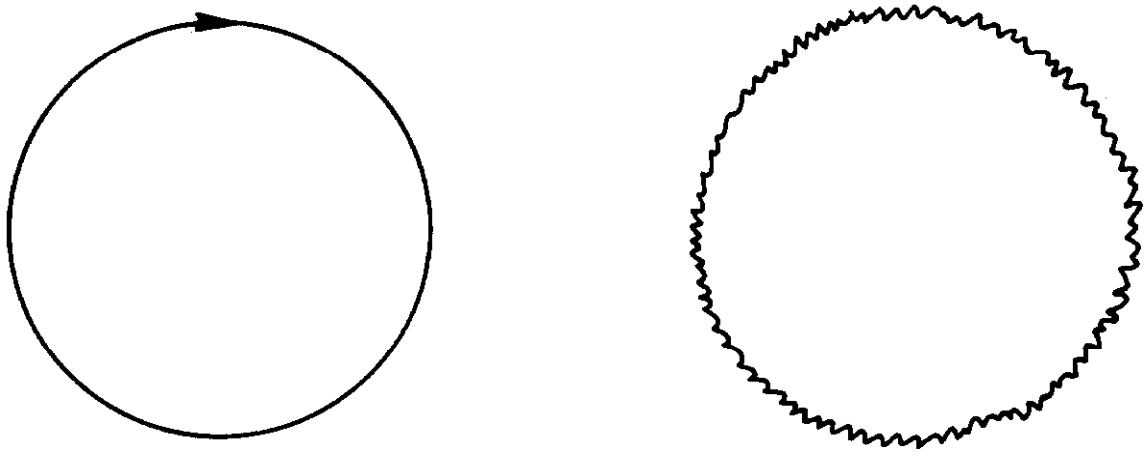

Figure 1

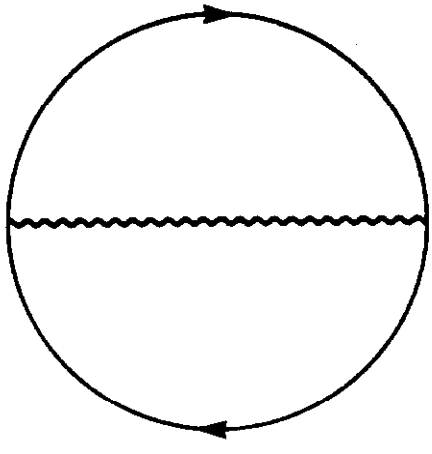

Figure 2

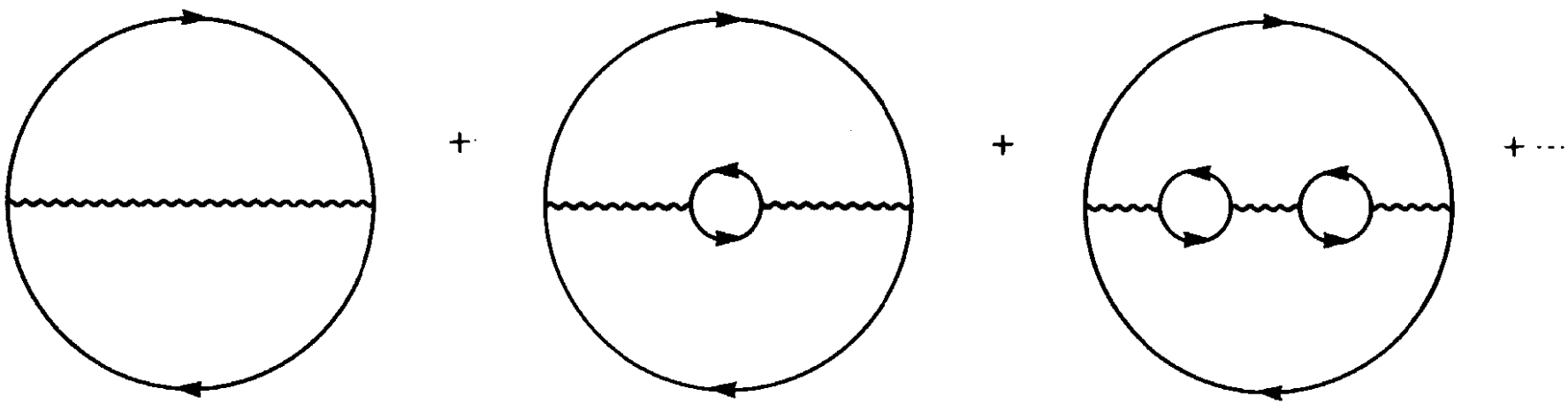

Figure 3

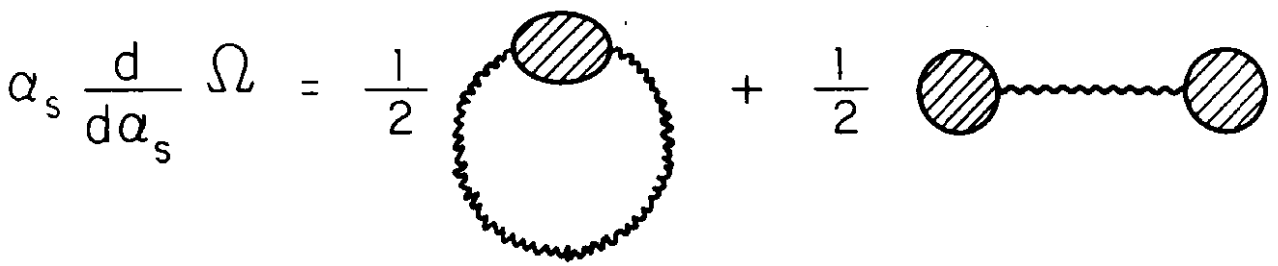

Figure 4

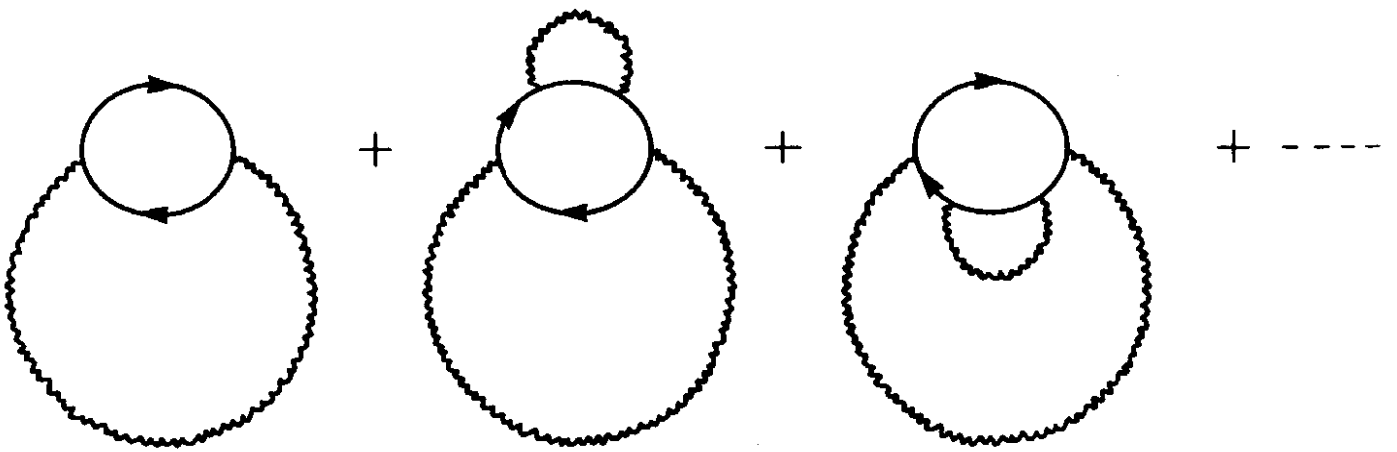

Figure 5

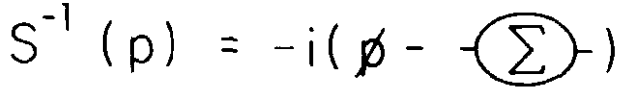

Figure 6

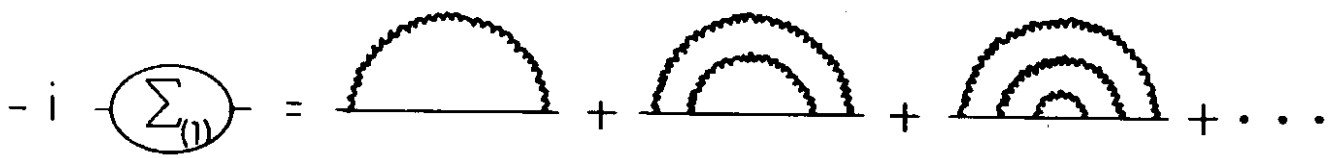

Figure 7

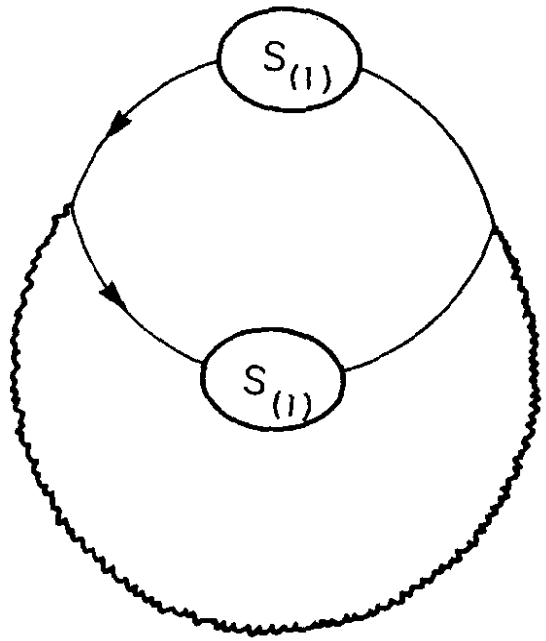

Figure 8

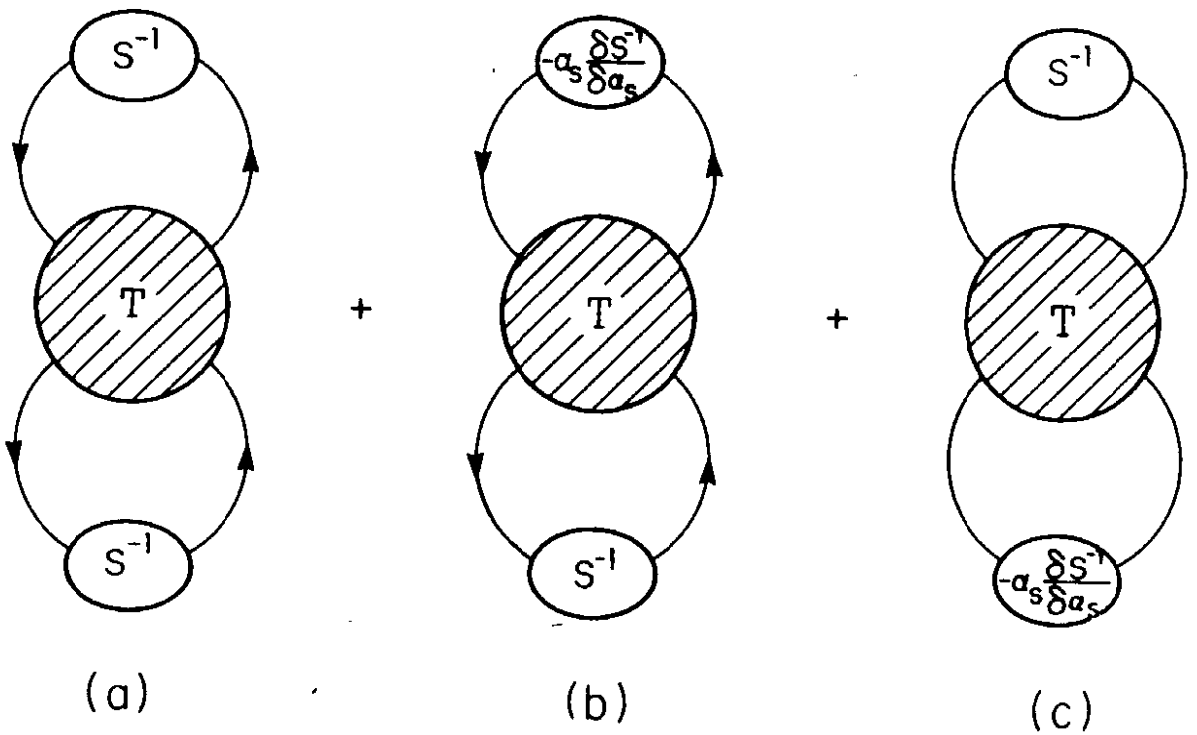
S^{-1}
T
S^{-1}
(a)
+
$-\alpha_s \frac{\delta S^{-1}}{\delta \alpha_s}$
T
S^{-1}
(b)
+
S^{-1}
T
$-\alpha_s \frac{\delta S^{-1}}{\delta \alpha_s}$
(c)

Figure 9

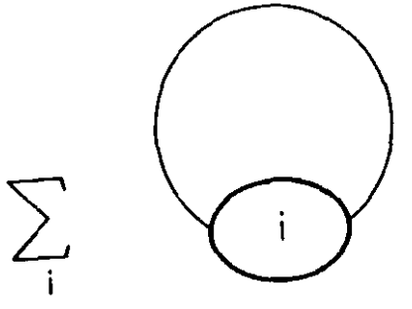

Figure 10

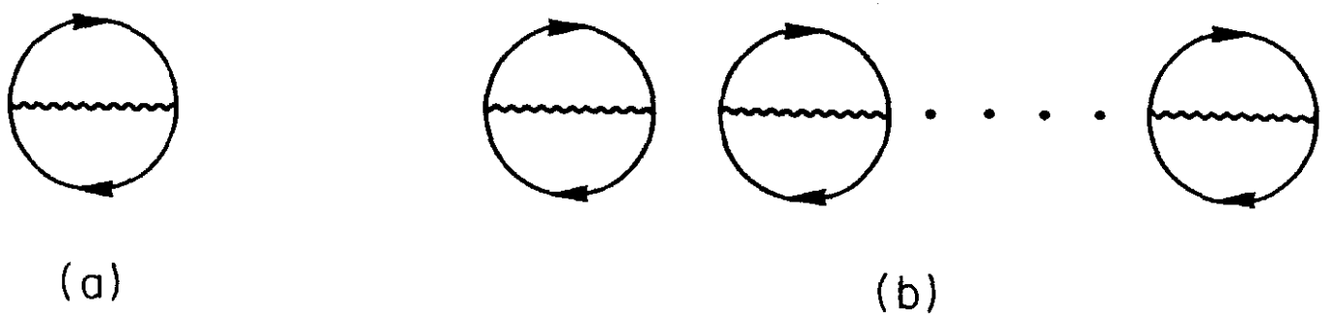

Figure 11

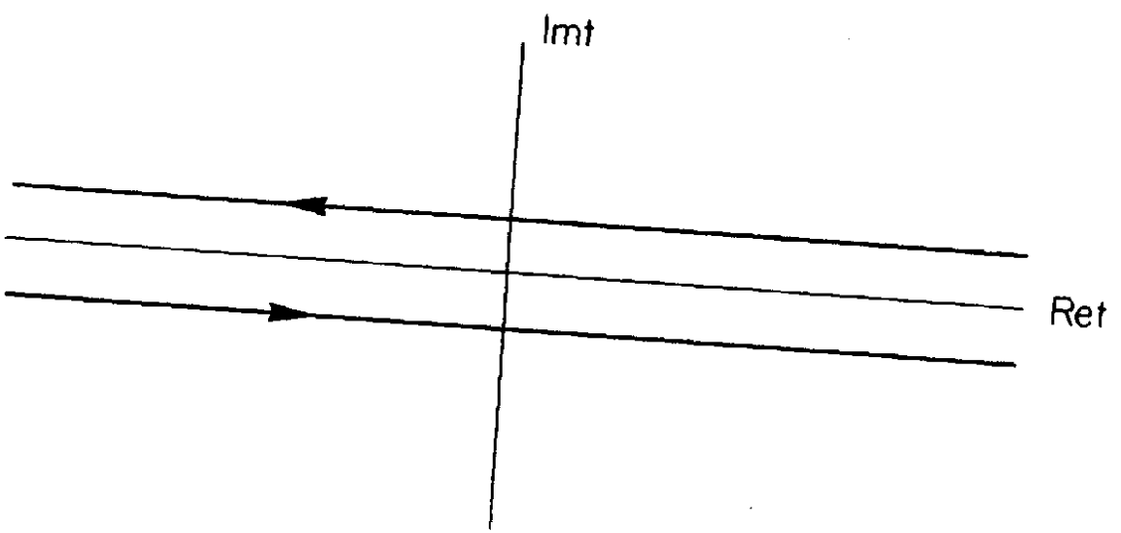

Figure 12

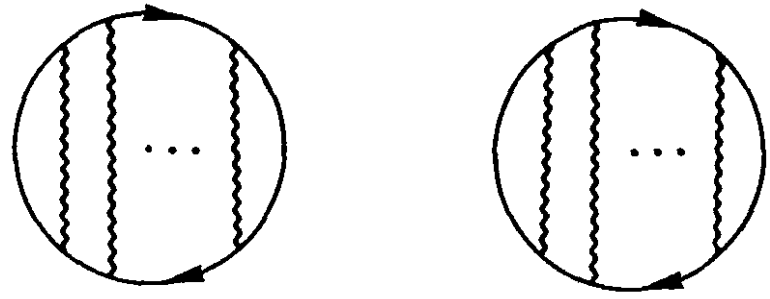

Figure 14

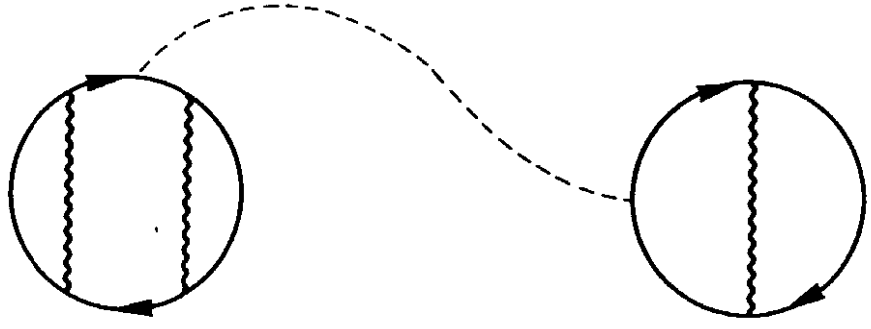

Figure 15

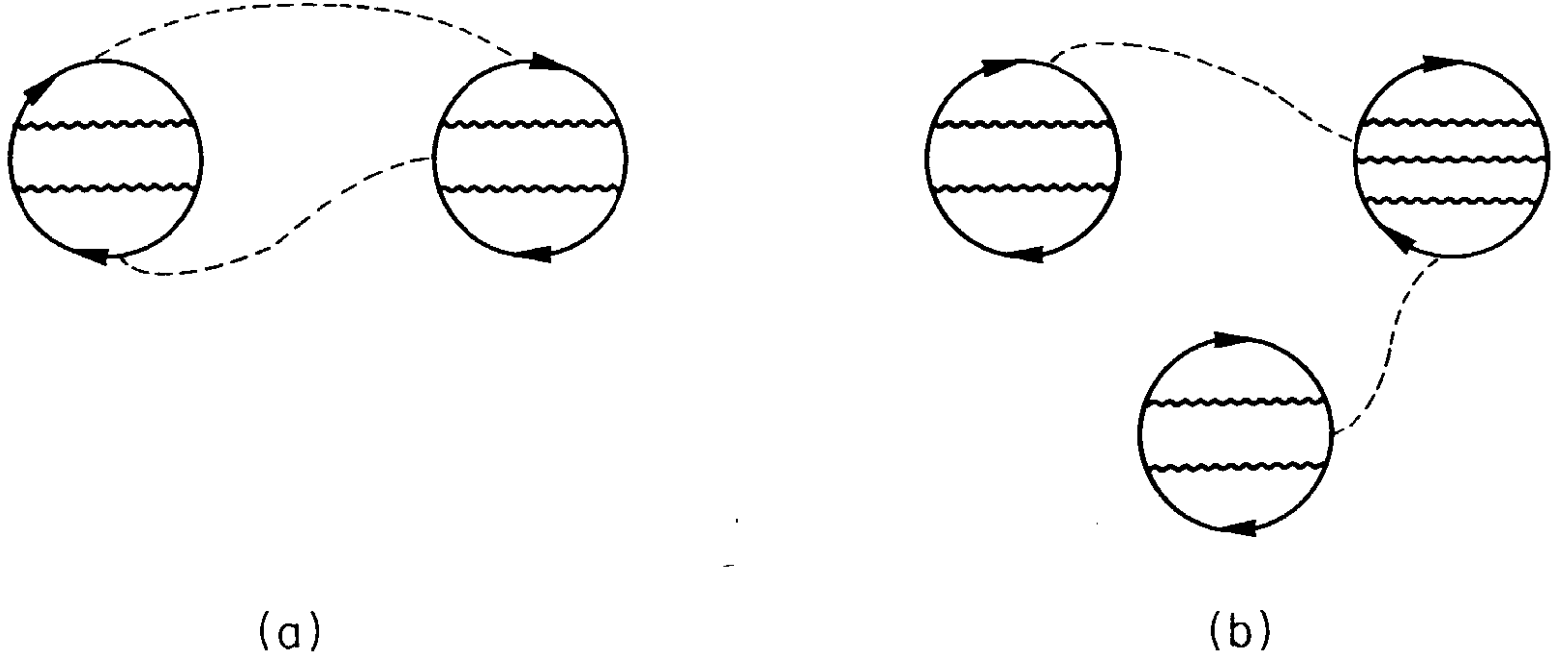

Figure 16

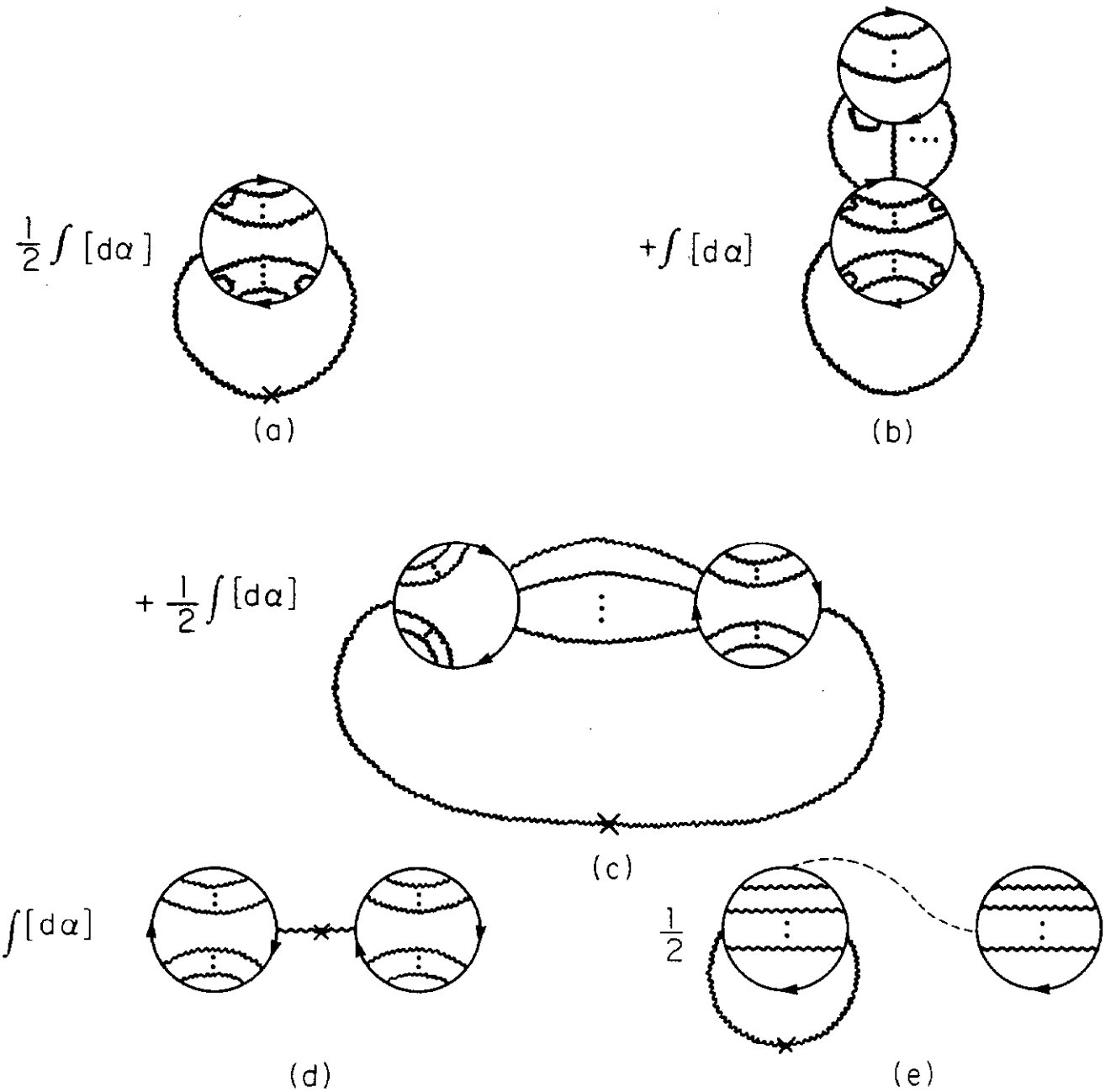
$\frac{1}{2}\int [d\alpha]$
(a)
$+\int [d\alpha]$
(b)
$+\frac{1}{2}\int [d\alpha]$
(c)
$+\frac{1}{2}\int [d\alpha]$
(d)
$\frac{1}{2}$
(e)

Figure 17

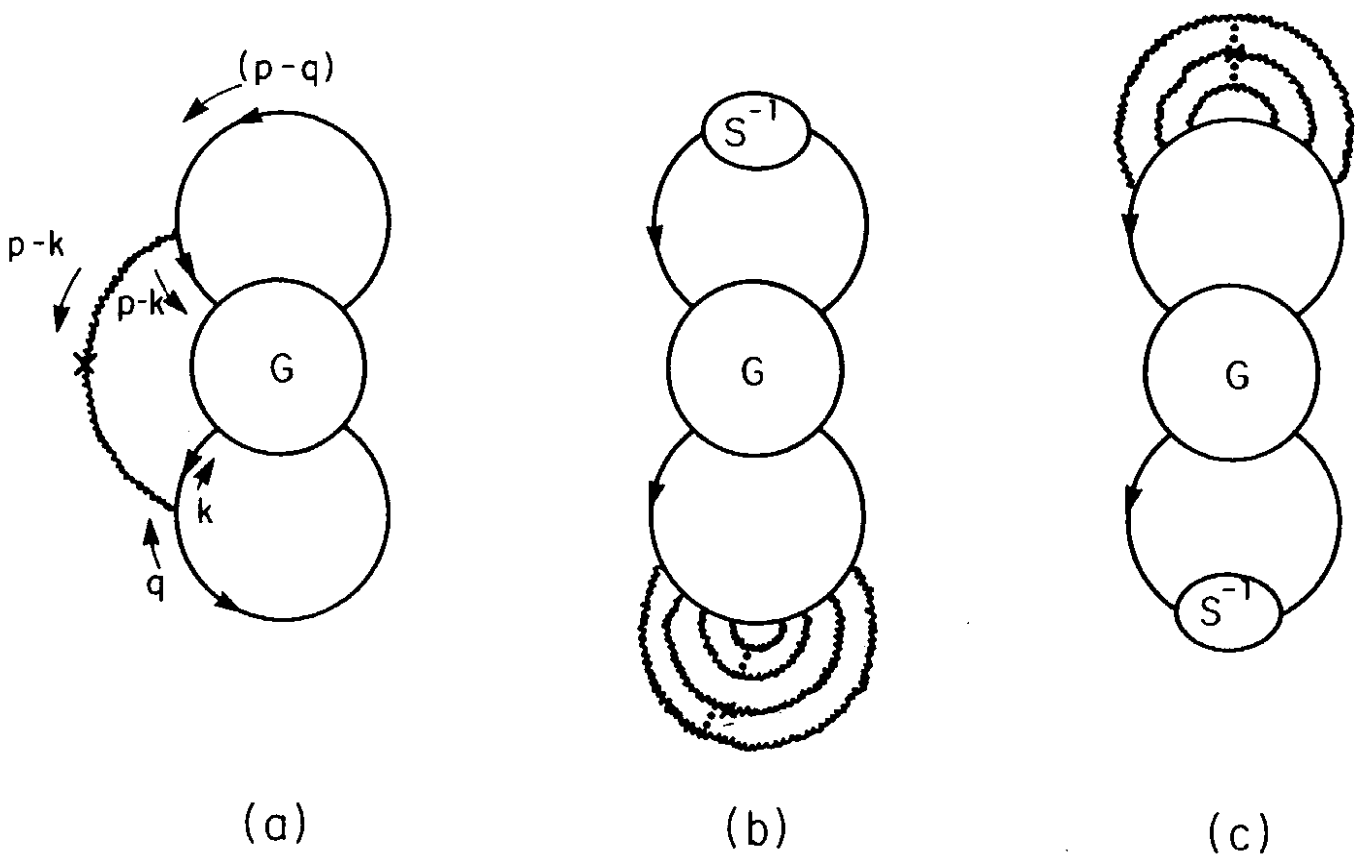

Figure 18

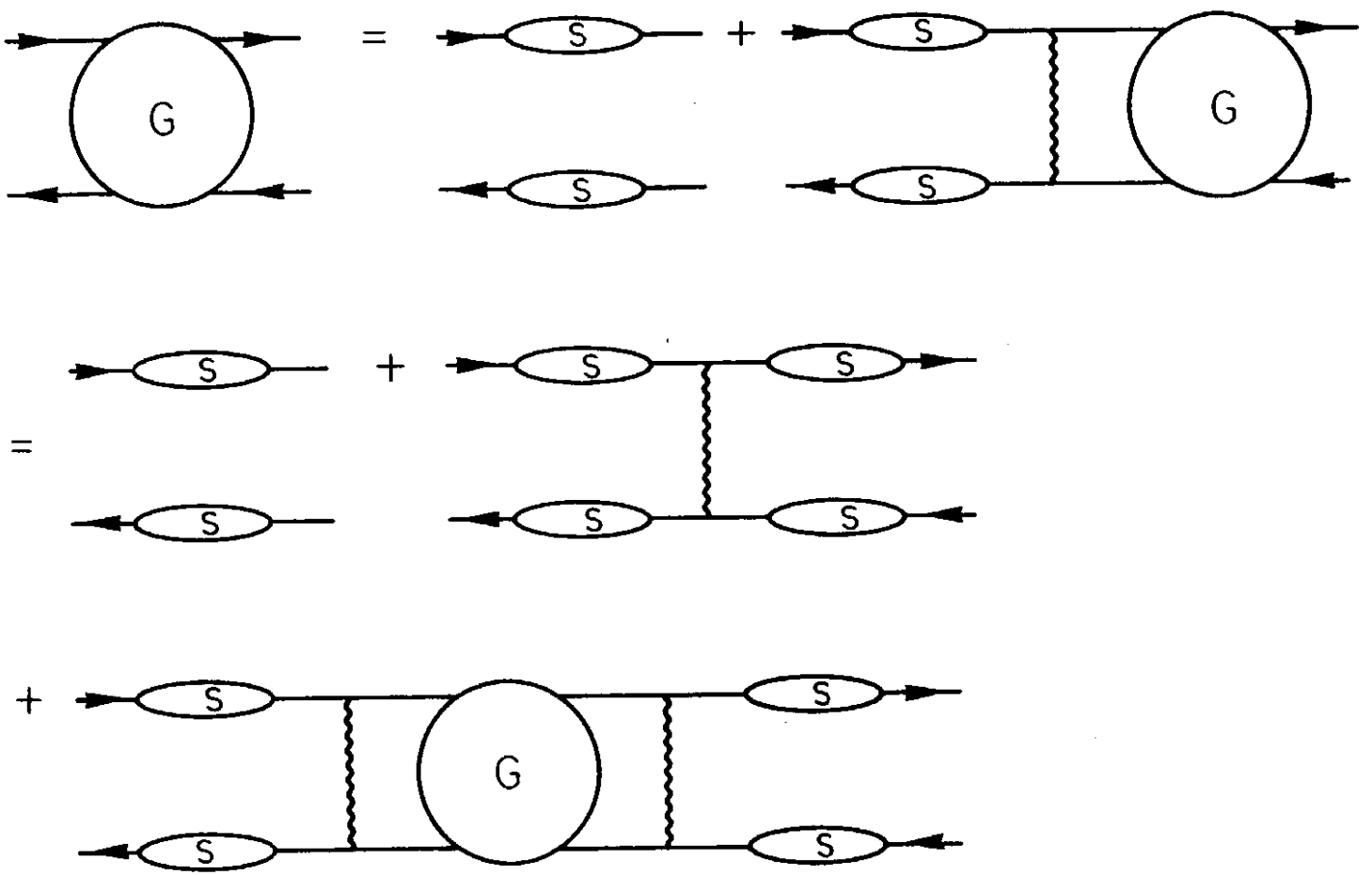

Figure 19